JOURNAL OF PETROLOGY | VOLUME 44 | NUMBER 5 | PAGES 937–965 | 2003

# Carbonatite and Alkaline Magmatism in Taourirt (Morocco): Petrological, Geochemical and Sr–Nd Isotope Characteristics

**C. WAGNER[1]*, A. MOKHTARI[2], E. DELOULE[3] AND F. CHABAUX[4]**

[1]LABORATOIRE DE PÉTROLOGIE, MODÉLISATION DES MATÉRIAUX ET PROCESSUS, LPMMP, UNIVERSITÉ UPMC, PARIS 6, 4 PLACE JUSSIEU, F-75252 PARIS CEDEX 05, FRANCE

[2]DÉPARTEMENT DE GÉOLOGIE, UNIVERSITÉ MOULAY ISMAIL, MEKNÈS, MOROCCO

[3]CENTRE DE RECHERCHES PÉTROGRAPHIQUES ET GÉOCHIMIQUES, CRPG, CNRS-UPR 23000, F-54501 VANDOEUVRE-LÈS-NANCY CEDEX, FRANCE

[4]CENTRE DE GÉOCHIMIE DE LA SURFACE, ECOLE ET OBSERVATOIRE DES SCIENCES DE LA TERRE, F-67084 STRASBOURG CEDEX, FRANCE

**RECEIVED FEBRUARY 6, 1999; ACCEPTED NOVEMBER 27, 2002**

*Alkaline lamprophyre dykes from Taourirt (North Morocco) contain numerous xenoliths, ranging from alkaline pyroxenites, kaersutitites, gabbros and nepheline syenites to a calcite carbonatite. The silicate xenoliths and the host rocks consist of Al- and Ti-rich diopside–salite, mica or kaersutitite, ± nepheline, ± plagioclase and K-feldspar, and ubiquitous apatite. Both the xenoliths and the lamprophyres are enriched in incompatible elements. The chemical composition of the lamprophyres cannot be accounted for by fractional crystallization alone. Moreover, the clinopyroxenes exhibit complex zoning, which requires repeated mixing of pulses of more or less fractionated melts. The carbonatite is a sövite cumulate with Sr-rich calcite, pyrochlore, fluorapatite, and rare salite. The Sr–Nd isotopic compositions of the Taourirt rocks indicate a depleted mantle source, the carbonatite having the most depleted composition, and define a linear trend similar to that of the East African carbonatites. The different rocks thus represent unrelated magmas, and the trend is interpreted as mixing between two components with HIMU and EM1 mantle end-member signatures. An EM2 mantle component could also be involved for a few samples; it may correspond to hydrous metasomatized mantle of the PP–PKP (phlogopite and phlogopite K-richterite peridotite) and MARID (mica, amphibole, rutile, ilmenite and diopside) type.*

KEY WORDS: *alkaline magmatism; carbonatite; Morocco; REE; Sr–Nd isotopes*

## INTRODUCTION

Carbonatites are frequently found together with alkaline silicate magmatic rocks of the melteigite–urtite series and nepheline syenites in alkaline–carbonatite complexes (e.g. Bell, 1998). The genesis of these complexes remains a matter of debate; commonly the carbonatites and associated nepheline-rich rocks are regarded as cogenetic (Le Bas, 1987; Beccaluva *et al.*, 1992), and experimental studies have demonstrated that carbonatites can be generated from parental carbonated silicate melts by crystal fractionation or carbonate–silicate immiscibility (e.g. Lee & Wyllie, 1998*a*, and references therein). However, carbonatites may also represent primary magmas derived from low degrees of partial melting of a carbonated peridotite mantle source (e.g. Sweeney, 1994; Wyllie & Lee, 1998; Lee *et al.*, 2000*b*). Moreover, the spatial association of carbonatites and silicate rocks does not

*Corresponding author: Telephone: 33 1 44 27 51 98. Fax: 33 1 44 27 39 11. E-mail: cw@ccr.jussieu.fr

*Journal of Petrology* 44(5) © Oxford University Press 2003; all rights reserved.

necessarily imply a genetic association, as shown by numerous complexes in which the Nd and Sr isotope compositions of the carbonatites and silicate rocks diverge significantly (Simonetti & Bell, 1994; Harmer & Gittins, 1998; Harmer, 1999).

At Taourirt (North Morocco) abundant dykes of alkaline lamprophyre have exhumed a suite of carbonate and alkaline silicate xenoliths (pyroxenites, nepheline syenites and gabbros). These rock types are similar to those encountered in alkaline igneous complexes worldwide, and would suggest the presence of a hidden alkaline–carbonatite complex beneath the area. Further, their study may provide insight into the possible links between carbonatites and alkaline silicate rocks.

In this paper we present petrographic, mineralogical and geochemical data (major and trace elements and Sr and Nd isotopes) for the main rock types. The objectives are (1) to assess the carbonatite nature of the carbonate xenolith, and (2) to discuss the petrogenesis of the various rocks, and the relationships, if any, between the carbonatite, the silicate xenoliths and the host lamprophyres.

## GEOLOGICAL SETTING

### Regional geology

The Taourirt region lies at the northeastern end of the Middle Atlas, Morocco (Fig. 1a). The Atlas structural domain is separated from the southern Precambrian to Palaeozoic Anti-Atlas domain by the South Atlasic fault, and from the Alpine Rif domain by the limit of the Tertiary thrust nappes to the north (Agard *et al.*, 1980). The Atlas domain consists of a Palaeozoic basement overlain by a post-Triassic cover divided in two structural regions, the Occidental and Oriental Meseta and the High and Middle Atlas Chain (Agard *et al.*, 1980). The Atlas Chain is a typical intracontinental chain whose polyphase tectonic evolution resembles that of pull-apart basins (Mattauer *et al.*, 1977; Laville, 1981). Its evolution was guided by inherited late Hercynian fractures and reflects both the opening of the North Atlantic Ocean and the following continental convergence induced by the northward motion of the African plate (Laville & Piqué, 1991).

The Taourirt area lies in the Tertiary–Quaternary Guercif–Oujda Basin, which represents a boundary zone between the folded Middle Atlas mountains Terni Mazgout and Beni Snassen to the north, and the tabular Horst Chain belonging to the Oriental Meseta to the south (Fig. 1a).

### The Taourirt magmatic rocks

The Taourirt igneous province mostly comprises alkaline lamprophyre (monchiquite and camptonite) sills and dykes intruding Jurassic sediments, mainly sandstone and rarely marl (Giret, 1985; Mokhtari, 1995). Olivine nephelinite lava flows and intrusions of alkaline pyroxenite and nepheline syenite also occur. The lamprophyres are late Cretaceous to Early Tertiary in age, based upon K–Ar determinations of $67 \pm 0{\cdot}2$ Ma (sample MJ1, A. Cheilletz, personal communication, 1998), and $57 \pm 3$ Ma (Charlot *et al.*, 1964) for lamprophyres from the Taourirt area. A few outcrops of alkaline rocks similar in nature and/or in age have been reported in North Morocco. Not far from Taourirt (75 km to the east), Hernandez *et al.* (1976) reported a $57 \pm 6$ Ma age for a basanite at Sidi Maatoug in the Rif unit. Further to the south (at 300 km from Taourirt) in the High Atlas, an alkaline–carbonatite complex has been described at Tamazert: it ranges from 44 to 35 Ma in age (Tisserant *et al.*, 1976; Harmand & Cantagrel, 1984), and consists of a series of alkaline intrusions and associated lamprophyre dykes, with both extrusive and intrusive carbonatites (Aghchmi, 1984; Bouabdli *et al.*, 1988; Bouabdli, 1993; Mourtada, 1997).

The alkaline lamprophyres and associated plutonic rocks from the Taourirt region were initially described by Duparc (1925) as aïounites (alkaline lamprophyres) and mestigmerites (pyroxenites and nepheline syenites). Figure 1b shows the main outcrops of alkaline rocks and the nature of the xenolithic materials. The sills and dykes of monchiquite and camptonite have a thickness of 0·5–4 m and may extend to several hundreds of metres in length. The lamprophyres locally form intrusive necks. Olivine nephelinite lava flows are mostly present in the eastern part of the Taourirt area (east of wadi Za). In some outcrops from the Koudiat Chmedda, the camptonite sills intrude the nephelinite, entraining nephelinite fragments, and therefore postdate the nephelinite. In the eastern part of the area (Koudiat Moujniba and Koudiat Chmedda; Fig. 1b) the alkaline lamprophyres and the nephelinites contain numerous mantle xenoliths; these include Al-augite nodules, Cr-diopside lherzolites, hydrous MARID suite xenoliths and K-richterite peridotites (Mokhtari & Velde, 1988; Wagner *et al.*, 1996). In contrast, monchiquites and camptonites from the west of wadi Za (Teniet El Amra and Djebel El Groun, Fig. 1b) contain abundant xenoliths of alkaline intrusive rocks: pyroxenites, kaersutitites, alkali gabbros and nepheline syenites. These xenoliths resemble some of the mestigmerites described by Giret (1985) from the area to the south of Teniet El Amra and Djebel El Groun (Fig. 1b) in a complex of alkaline silicate rocks including pyroxenites and nepheline syenites, which intrude volcanic breccias and are cross-cut by alkaline lamprophyre dykes. Nearby, a carbonatite inclusion has been found in a camptonite dyke (Mokhtari *et al.*, 1996).

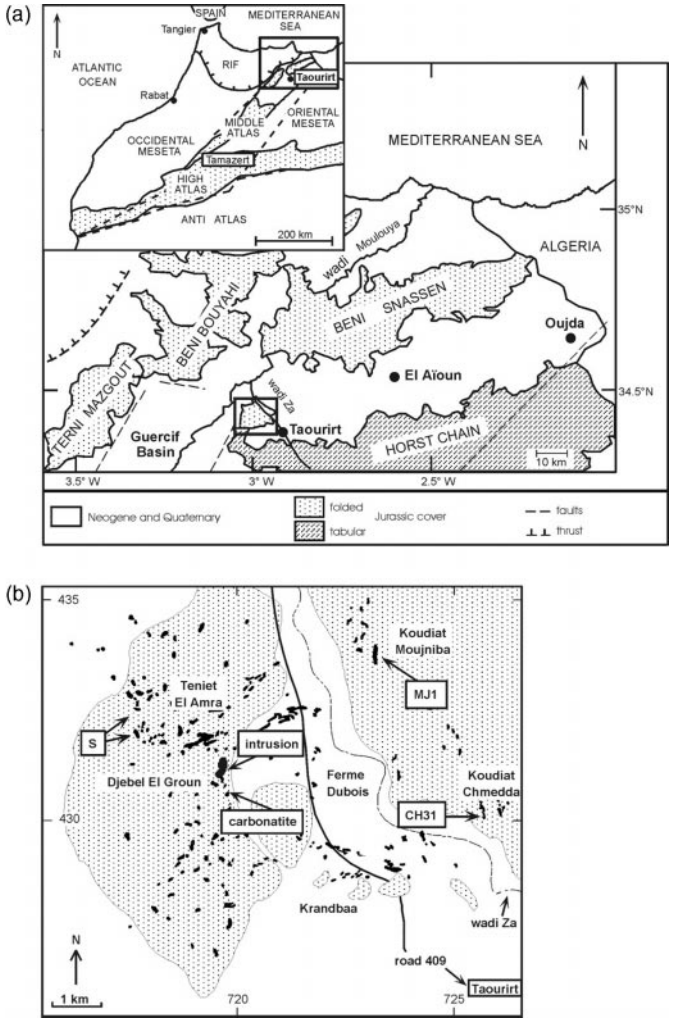


**Fig. 1.** (a) Simplified map of Morocco showing the main tectonic units and expanded view of the Taourirt–Oujda area. (b) Detailed map of the studied region showing the distribution of the alkaline rocks [modified after Agard (1950) and Mokhtari & Velde (1988)], which mostly crop out through the Jurassic folded cover (stippled field). The four main sampling regions are Teniet El Amra, Djebel El Groun, Koudiat Moujniba and Koudiat Chmedda. In Teniet El Amra and Djebel El Groun, camptonites and monchiquites (marked 'S' on the map) contain the various alkaline silicate xenoliths of this study. The lamprophyres also contain rare fragments of peridotitic material (xenocrysts of Cr-diopside and Cr-spinel included in olivine). The complex intrusion of pyroxenites and nepheline syenites ('intrusion') studied by Giret (1985) crops out in Djebel El Groun. The carbonatite inclusion ('carbonatite') was found in a camptonite dyke nearby. In Koudiat Moujniba and Koudiat Chmedda, monchiquites (e.g. sample MJ1), camptonites and olivine nephelinite (observed only at Chmedda, e.g. sample CH31) host numerous small fragments of Al-augite and Cr-diopside xenoliths and metasomatized xenoliths or xenocrysts of K-richterite peridotites and MARID rocks (Wagner *et al.*, 1996), and rare zoned clinopyroxenes of the type abundant in the alkaline rock xenoliths from Teniet El Amra and Djebel El Groun. Literature data for these four regions plus the Ferme Dubois location and Krandbaa were used for comparison. In the Ferme Dubois location, lamprophyres contain xenocrysts of peridotitic olivine as well as zoned clinopyroxenes as documented above. In Krandbaa, lamprophyres and olivine nephelinites contain xenoliths of alkaline pyroxenite and xenocrysts from disaggregated peridotite (more abundant in the olivine nephelinites).

This study is limited to occurrences around the Ferme Dubois locality, an area limited by $x = 715$–$725$ and $y = 425$–$435$ on the detailed map of Morocco (Taourirt sheet 1/50 000; Giret, 1985), and mainly focuses on the carbonate and silicate xenoliths, and on the host alkaline lamprophyres from the Teniet El Amra and Djebel El Groun area (Fig. 1b).

## ANALYTICAL METHODS

Electron microprobe analyses were performed using a Cameca CAMEBAX SX 50 wavelength-dispersive system at the Centre d'Analyses CAMPARIS, University Paris 6. The operating conditions were accelerating voltage 15 kV, beam current 40 nA for oxides, olivines and pyroxenes, and 10 nA for

amphiboles and mica; counting times were never less than 20 s on each peak, and a PAP matrix correction program (Pouchou & Pichoir, 1985) was employed. Standards were synthetic metal oxides and natural minerals.

Whole-rock samples of the carbonate xenolith, one kaersutitite, two pyroxenites, two gabbros, one nepheline syenite, one carbonate-rich xenolith, seven lamprophyres and one olivine nephelinite were crushed in acid-cleaned agate mortars to minimize contamination. Major elements were measured by X-ray fluorescence (XRF) at the Laboratory of Petrology, University Paris 6, on fused glass discs, except MnO, $Na_2O$, $K_2O$ and $P_2O_5$, which were analysed by inductively coupled plasma atomic emission spectrometry (ICP-AES) at the École Nationale Supérieure des Mines de Saint-Étienne (ENSMSE), France. The trace elements Sc, V, Cr, Co, Ni, Cu, Zn and Nb were determined by ICP-AES at ENSMSE, and Rb, Sr, Zr, Hf, Y, Ba, Th, U and rare earth elements (REE) by inductively coupled plasma mass spectrometry (ICP-MS) at the University of Montpellier, France (for the xenoliths), and the Centre de Géochimie de la Surface (CGS), Strasbourg, France (for the host rocks). The basalt BEN from GIT-IWG (Govindaraju, 1989) was used as standard. Accuracy is ±10%.

The same xenolith and olivine nephelinite samples and two lamprophyres were analysed for their Sr and Nd isotope composition, using a VG Sector mass spectrometer equipped with a five-cup multicollector, at the CGS. The analytical procedure has been described in detail by Steinmann & Stille (1997) and Tricca *et al.* (1999). About 50–100 mg of rock powder was digested in a $HF–HNO_3–HClO_4$ mixture. Sr and REE fractions were separated by cation exchange chromatography with ammonium citrate and eluted with HCl. Nd purification from the remaining REE fraction was carried out using cation exchange resin and α-hydroxyisobutyric acid as the eluent. For mass spectrometric measurement Sr was loaded with nitric acid and a $Ta_2O_5$ activator on a single W filament. The ratio $^{86}Sr/^{88}Sr = 0{\cdot}1194$ was used for fractionation correction. Typically 100 scans were collected to achieve a precision of about $2 \times 10^{-5}$. During the period of study, repeated analysis of the NBS 987 Sr standard yielded an average $^{87}Sr/^{86}Sr = 0{\cdot}710258 \pm 14$ (2 standard deviations of the mean, $n = 8$). Nd was measured using the Ta–Re double filament method (Tricca *et al.*, 1999). The ratio $^{146}Nd/^{144}Nd = 0{\cdot}7219$ was used for fractionation correction. During the period of measurement, the average $^{143}Nd/^{144}Nd$ ratio for the La Jolla Nd standard was $0{\cdot}511855 \pm 8$ (2 standard deviations of the mean, $n = 5$).

Eighteen clinopyroxenes were selected from the xenolith and lava samples analysed above or from rock types similar to the ones analysed. *In situ* REE and trace element analyses were performed on the clinopyroxenes using the CRPG-Nancy CAMECA IMS-3f ion microprobe. The analytical conditions are similar to those of Chabiron *et al.* (2001), using the pyroxene glass standard A5O. The analytical precision and reproducibility for the various elements range between 10 and 20%.

## PETROGRAPHY AND MINERALOGY

### The silicate rocks

*Host camptonites and monchiquites*

The petrography and the mineralogy of the alkaline lamprophyres from the Taourirt area have been described previously (Giret, 1985; Mokhtari & Velde, 1988; Mokhtari, 1995; Wagner *et al.*, 1996) and are therefore only summarized briefly here (Table 1). Apart from frequently zoned clinopyroxene, the major phenocryst phases are kaersutite in the camptonites, and biotite (± minor kaersutite) in the monchiquites. Representative electron microprobe analyses of clinopyroxene, amphibole and mica are given in Table 2. Plagioclase and alkali feldspar frequently coexist. Ti-magnetite is common, and partly altered olivine and haüyne are present in some samples; apatite, rare titanite and perovskite are accessories. The groundmass is frequently altered and consists of a low-temperature assemblage of zeolites, which probably replace feldspar ± nepheline. The rocks typically exhibit a globular structure (millimetre size) of leucocratic spherical or more irregularly shaped ocelli composed of calcite and analcite, and feldspathic segregations in some of the more evolved camptonites (Table 1). Such textures are common in lamprophyres but their origin is much debated (Rock, 1991). Abundant xenocrystic material includes clinopyroxene, amphibole, mica, and spinel.

*Olivine nephelinites*

These lavas comprise millimetre-sized phenocrysts of magnesian ($Fo_{88}$) NiO-rich (0·3 wt %) olivine (10% by volume), $Al_2O_3$- and $TiO_2$-rich (7·4–11·4 and 3·6–5·8 wt %, respectively) diopside (54%), rare (2%) $TiO_2$-rich (up to 7 wt %) phlogopite and large (up to 400 μm) crystals of nepheline (15%). In the groundmass analcite forms poikilitic patches including diopside, abundant phlogopite, Ti-magnetite and rare apatite. Details of the mineral compositions have been given by Wagner *et al.* (1993).

*Table 1: Major phase mineralogy (except clinopyroxene, detailed in Fig. 4) of lamprophyres and silicate xenoliths from Taourirt*

| | Phenocrysts and microphenocrysts | Relict phases | Leucocratic structures |
|---|---|---|---|
| Host lamprophyres | *amp* (53–69), $TiO_2$ = 4·5–6·1 wt % | *amp* core (43–49), $TiO_2$ = 4·4–5·3 wt % | *type 1*: zoned ocelli: with rounded analcite core + calcite ± felds ($Or_{89}$) rim |
| (S2 to S6, 93·11) | *mica* (75–80), $TiO_2$ = 6·2–9·7 wt %, BaO = 1·7–3·0 wt % | *biotite* core (59–61), $TiO_2$ = 4·4–4·6 wt %, BaO = 0·6–0·8 wt % | *type 2*: unzoned ocelli: calcite + analcite ± felds ($Or_{95}$) ± chabazite ± chlorite |
| | *plag* ($An_{24-48}$) + *felds* ($Or_{47-97}$) | | *type 3*: irregularly shaped ocelli + veins Sr-rich (1·7 oxide wt %) calcite ± analcite ± magnetite ± celestite |
| | | | *type 4*: segregations: Sr-bearing (1–2 oxide wt %) plag ($An_{16-37}$) |
| Pyroxenites | *amp* (52–73), $TiO_2$ = 4·1–6·9 wt % | | rarer than in host lamprophyres |
| (THC, THD, TH4, S41, | *mica* (62–78), $TiO_2$ = 4·8–7·0 wt %, | *biotite* core (49–58), $TiO_2$ = 3·8–5·7 wt %, | type 1 and 2 ocelli |
| S42, ES) | BaO = 0·5–3·0 wt % | BaO = 0·1–2·3 wt % | |
| | not ubiquitous *felds* ($Or_{52-69}$ and $Or_{85-98}$) | | |
| Kaersutitites | *amp* (67–68), $TiO_2$ = 4·8–4·9 wt % | | |
| (Db, S4k) | *mica* (73–75), $TiO_2$ = 6·5–6·8 wt %, BaO = 0·4–0·8 wt % | | |
| Nepheline syenites | *mica* (36–52), $TiO_2$ = 2·1–3·0 wt %, | xenocrystic (?) *amp* (65–67), | rarer than in host lamprophyres |
| (NS, S4) | BaO < 0·2 wt %, MnO up to 1 wt % | $TiO_2$ = 4·7–5·1 wt % | type 1 ocelli (± hematite) |
| | *felds* ($Or_{47-64}$) | | |
| | *neph* $Ne_{77-80}$ $Ks_{14-17}$ $Qz_{3-8}$ | | |
| Alkali gabbros | *amp* (47–57), $TiO_2$ = 4·1–5·6 wt % | | |
| (S43, Sc) | *mica* (51–59), $TiO_2$ = 4·9–6·1 wt %, BaO = 0·1–0·9 wt % | | |
| | *plag* ($An_{34-48}$) | | |
| Syenites (S922) | *mica* (36–50), $TiO_2$ = 2–3 wt %, | xenocrystic *amp* (51), | |
| | BaO < 0·2 wt % | $TiO_2$ = 4·4 wt % | |
| | *felds* ($Or_{41-57}$) | | |

All numbers in parentheses represent mg-number = 100 Mg/(Mg + $Fe_{total}$). *amp*, kaersutite; *plag*, plagioclase; *felds*, alkali feldspar; *neph*, nepheline.

### *Alkaline silicate xenoliths*

These xenoliths range in size from a few centimetres to 30 cm in diameter. The main rock types are alkali pyroxenite, nepheline syenite, kaersutitite, and less abundant alkali gabbro and syenite. Representative modal compositions are given in Table 3. The major phases are clinopyroxene, amphibole ± mica, plagioclase, K-feldspar and nepheline. The clinopyroxenes are Al- and Ti-rich diopside or salite. Micas are Ti-rich phlogopite or biotite. Some phlogopite crystals show a relict biotite core. Amphibole is kaersutite and is highly magnesian [up to mg-number = 73; mg-number =100 Mg/(Mg + $Fe_{total}$)] in the pyroxenites and the kaersutitites, but richer in Fe (mg-number 52–57) in the alkali gabbros. Feldspars are present in most xenoliths: K-rich alkali feldspar in the pyroxenites and plagioclase in the alkali gabbros. Nepheline is completely altered in the pyroxenites but fresh in the nepheline syenites. The mineral compositions are summarized in Table 1.

*Pyroxenites.* Micaceous pyroxenites and melteigites are the dominant xenolith type, whereas amphibole-rich pyroxenites are less common. Both types consist mainly of zoned clinopyroxene, mica, variable amounts of kaersutite, nepheline and rare alkali feldspar; Ti-magnetite, apatite and titanite are ubiquitous accessory phases. Calcite is common either as an interstitial

*Table 2: Representative electron microprobe analyses of minerals in the host lamprophyres: clinopyroxene and amphibole from camptonite S6 and micas from monchiquite S3*

| | CPX | | | AMP | | MICA | |
|---|---|---|---|---|---|---|---|
| | 1 | 2 | 3 | 4 | 5 | 6 | 7 |
| $SiO_2$ | 46·07 | 41·75 | 45·87 | 38·08 | 37·86 | 35·08 | 35·35 |
| $Al_2O_3$ | 6·65 | 10·52 | 6·30 | 13·32 | 13·29 | 16·60 | 15·27 |
| $TiO_2$ | 2·75 | 3·89 | 1·77 | 6·04 | 4·37 | 6·15 | 4·68 |
| FeO* | 7·96 | 10·72 | 13·33 | 11·14 | 18·48 | 8·27 | 16·38 |
| MgO | 11·59 | 8·23 | 8·22 | 11·55 | 7·93 | 17·93 | 13·27 |
| MnO | 0·17 | 0·28 | 0·50 | 0·24 | 0·49 | 0·17 | 0·28 |
| CaO | 22·79 | 22·20 | 21·36 | 11·94 | 10·96 | | |
| $Na_2O$ | 0·73 | 1·01 | 1·55 | 2·33 | 2·17 | 0·53 | 0·51 |
| $K_2O$ | | | | 1·95 | 1·86 | 8·83 | 9·22 |
| BaO | | | | | | 2·12 | 0·85 |
| F | | | | 0·37 | 0·06 | 0·55 | 0·36 |
| Cl | | | | 0·04 | 0·04 | 0·02 | 0·02 |
| Total | 98·69 | 98·60 | 98·90 | 96·83 | 97·47 | 96·01 | 96·03 |
| $Fe_2O_3$ | 4·24 | 5·98 | 7·34 | | | | |
| FeO | 4·14 | 5·34 | 6·73 | | | | |
| *Cations per formula unit* | | | | | | | |
| Si | 1·741 | 1·601 | 1·759 | 5·768 | 5·863 | 5·162 | 5·358 |
| Al | 0·296 | 0·476 | 0·285 | 2·381 | 2·428 | 2·879 | 2·728 |
| Ti | 0·078 | 0·112 | 0·051 | 0·687 | 0·509 | 0·681 | 0·533 |
| $Fe^{3+}$ | 0·121 | 0·173 | 0·211 | | | | |
| $Fe^{2+}$ | 0·131 | 0·171 | 0·217 | 1·410 | 2·394 | 1·018 | 2·076 |
| Mg | 0·653 | 0·471 | 0·469 | 2·607 | 1·829 | 3·932 | 2·997 |
| Mn | 0·005 | 0·009 | 0·016 | 0·031 | 0·064 | 0·021 | 0·036 |
| Ca | 0·922 | 0·912 | 0·877 | 1·938 | 1·818 | | |
| Na | 0·053 | 0·075 | 0·115 | 0·684 | 0·651 | 0·151 | 0·150 |
| K | | | | 0·378 | 0·367 | 1·658 | 1·783 |
| Ba | | | | | 0·122 | 0·050 | 0·013 |
| F | | | | 0·177 | 0·029 | 0·256 | 0·173 |
| Cl | | | | 0·010 | 0·010 | 0·004 | 0·005 |
| mg-no. | 72·2 | 57·8 | 52·3 | 64·9 | 43·3 | 79·6 | 59·0 |

Clinopyroxene (CPX): 1, phenocryst; 2, microcryst, 3, green core. Kaersutite (AMP): 4 and 5, dark relict core. MICA: 6 and 7, biotite relict core. Formulae calculated on 6 (cpx), 22 (mica) and 23 (amphibole) O atoms. mg-no. = 100Mg/(Mg + Fetotal). Total minus F, Cl = O for AMP and MICA. No Cr was detected.
*Total iron expressed as FeO.

phase or in ocelli. The xenoliths exhibit large variations in modal mineralogy (Table 3), texture and grain size. Fine- and coarse-grained pyroxenites have been observed: for example, sample ES (Fig. 2a) is a fine-grained (200 μm average grain size) rock that contains subhedral clinopyroxene and mica, interstitial alkali feldspar, Ti-magnetite and rare apatite. Large (millimetre grain size) poikilitic amphibole crystals are present in one part of the specimen; they contain numerous clinopyroxene crystals and rare mica, Ti-magnetite and cloudy apatite. Sample S42 (Fig. 2b) is coarse grained (millimetre grain size), with euhedral to subhedral zoned clinopyroxene, mica and altered nepheline (replaced by zeolite), and smaller (100 μm) apatite included in clinopyroxene and mica. This sample does not contain either feldspar or amphibole, whereas large euhedral to subhedral prismatic crystals of amphibole may be present in other coarse-grained samples. Large crystals of titanite occur, which have a destabilized rim of secondary

*Table 3: Mineralogical composition and modal proportion (expressed in volume %) for representative xenoliths: melteigites (M), pyroxenites (P), kaersutitite (K), alkali gabbros (G), syenite (S) and nepheline syenite (NS)*

| | M | | P | | K | G | | S | NS |
|---|---|---|---|---|---|---|---|---|---|
| | S42 | TH4 | S41 | ES | Db | S43 | Sc | 922 | S4 |
| Cpx | 40·5 | 46·8 | 36·8 | 50·6 | 23·7 | 2·6 | | 0·7 | 1·8 |
| Mica | 40·3 | 6·6 | 0·6 | 25·6 | 0·2 | | 10·5 | 3·6 | 2·2 |
| Amp | tr | 9·0 | 42·3 | 14·9 | 69·0 | 40·6 | 37·2 | 8·9 | 16·2 |
| Neph | 11·7 | 28·9 | 19·2* | | | | | | 34·7 |
| Felds | | | | 2·0 | | 48·9 | 51·4 | 85·9 | 30·9 |
| Apat | 1·2 | 0·8 | 0·5 | 2·1 | tr | 1·8 | 0·9 | tr | 0·3 |
| Titanite | | 2·1 | 0·3 | | | | | 0·9 | 3·2 |
| Mt | | | 0·3 | 4·8 | 7·1 | 0·2 | tr | | |
| Alter | 6·3 | 5·8 | | | | 5·9 | | | 10·7 |

Amp, amphibole; Neph, nepheline; Felds, feldspar; Apat, apatite; Mt, magnetite; Alter, undefined alteration products; tr, trace.
*Altered nepheline and feldspar.

perovskite at the contact with the nepheline. Calcite-rich ocelli have also been observed in some samples. Fresh nepheline has never been observed in the pyroxenites.

*Kaersutitites*. In a similar way to the pyroxenites, these samples occur as both fine- and coarse-grained varieties. The fine-grained types may exhibit a well-developed trachytic texture defined by flow-aligned amphibole grains (sample S4k, Fig. 2c), whereas the coarser types have large (millimetre-sized) euhedral crystals of amphibole, smaller (100–400 μm grain size) diopside and titanite, with interstitial patches of calcite and altered material (mostly zeolites). Composite nodules have been found with an inner coarse-grained pyroxenite core, sharply separated from surrounding fine-grained kaersutitite. The coarse-grained sample Db (Fig. 2d) shows a typical cumulate texture of kaersutite and Ti-magnetite, and intercumulate small diopside and rare altered haüyne or nosean. Phlogopite is occasionally included in the kaersutite crystals. Some 120° triple junctions are observed between amphibole or pyroxene grains.

*Nepheline syenites*. These are coarse grained (500 μm grain size) and consist of euhedral to subhedral nepheline (typically replaced by micaceous alteration products and cancrinite at the margins), altered former haüyne or nosean, and alkali feldspar (Fig. 2e). Rare kaersutite crystals are rimmed by a thick altered opaque zone and sometimes replaced by mica. Small fresh salite crystals, pyrochlore and titanite are observed in the interstitial altered material. Rounded calcite-rich ocelli have been observed. Composite nodules have been found with an inner core of coarse-grained pyroxenite surrounded by a nepheline syenite with a sharp contact between them, and no reaction zone. The nepheline syenite includes some fragments of the pyroxenite, clearly indicating that it postdates the pyroxenite.

*Amphibole-bearing alkali gabbros*. All samples contain abundant kaersutite with minor and variable amounts of mica and clinopyroxene. Sample Sc is a large (30 cm in size) heterogeneous xenolith in terms of texture and grain size and shows two distinct but not sharply separated parts: first, a coarse-grained (millimetre-sized crystals) part (Scb) showing a sub-ophitic texture of plagioclase laths and kaersutite crystals, and rare mica. This part is enriched in plagioclase laths towards its contact with the second part of the xenolith where a 2 mm wide leucocratic zone has developed. This second melanocratic part (Scn) is fine grained (100–200 μm grain size) and comprises kaersutite, plagioclase, large mica crystals and some rare alkali feldspar. In both parts, olivine has been observed only as rare relict cores surrounded by a complex aggregate of small clinopyroxene, magnetite and radial mica laths. The mineral composition is similar in the two parts and falls within the range of compositions observed in other gabbro samples (Table 1). No evident chronological relationship can be deduced from the hand specimen or from microscopic-scale observations.

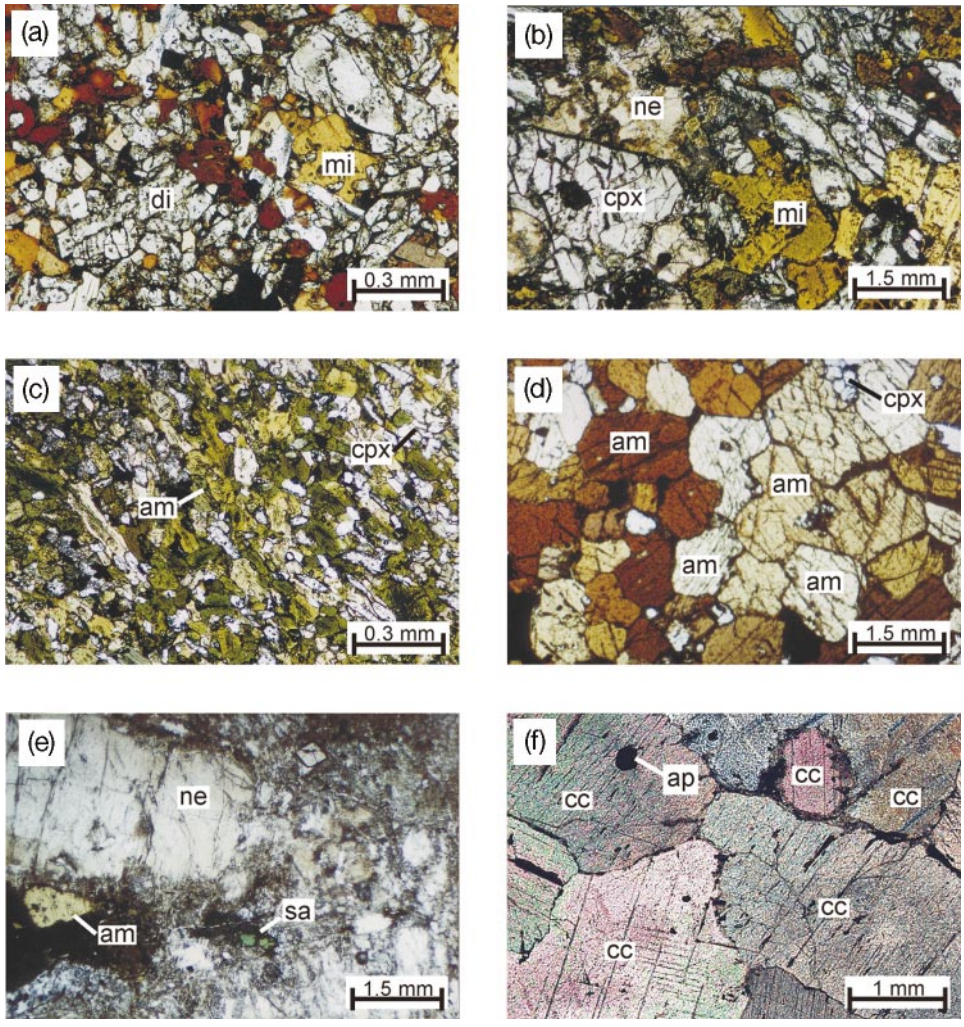


**Fig. 2.** Photomicrographs of representative xenoliths from Taourirt. (a) Fine-grained pyroxenite (ES) with biotite and diopside. (b) Coarse-grained pyroxenite (S42) with large subhedral clinopyroxene (colourless diopside and light green salite), biotite and altered nepheline (light yellow). (c) Fine-grained kaersutitite (S4k) with flow-aligned brown-green amphibole crystals and colourless clinopyroxene. (d) Coarse-grained kaersutitite Db with a cumulate texture; a few colourless diopside grains are observed between the cumulate amphiboles. (e) Coarse-grained nepheline syenite (NS) showing euhedral to subhedral nepheline with a fresh core, small green salite and a large destabilized kaersutite crystal with a well-developed outer dark rim. (f) Carbonate xenolith showing the subhedral millimetre-sized calcite grains. The apatite included in a calcite grain should be noted (crossed nicols photomicrograph). di, diopside; sa, salite; cpx, clinopyroxene; mi, mica; am, amphibole; ne, nepheline; ap, apatite; cc, calcite.

*Syenites*. These samples contain alkali feldspar, destabilized kaersutite rimmed by a dark reaction zone, and rare clinopyroxene.

*Carbonate-rich xenoliths*. Carbonates form ocelli, veinlets and pervasive patches, which are heterogeneously distributed throughout the samples (ES2, ES7). The carbonate-rich parts may contain rare crystals of salite and aegirine (e.g. in sample ES7), apatite, allanite, zircon, and baddeleyite, whereas altered alkali feldspar, destabilized mica and salite, apatite, rare andradite garnet and relict diopside are found in the silicate parts. The salite displays a wide range in mg-number (21–56), and differs in the silicate and the carbonate-rich parts: the salite from the carbonate-rich parts is less magnesian (mg-number 21–45) than that from the silicate parts (mg-number 36–56). It also has lower $Al_2O_3$ and higher $Na_2O$ (0·1–1·0 wt % and 2·0–7·8 wt %, respectively, compared with 0·9–3·0 wt % and 1·6–4·2 wt %, respectively). The low SrO content (<1·0 wt %) of the apatite and the Sr-free calcite of the ocelli are distinct from apatite and calcite in the magmatic carbonatites. K-rich feldspars ($Or_{73–74}$) are surrounded by albite ($Ab_{74}$) at the contact with the

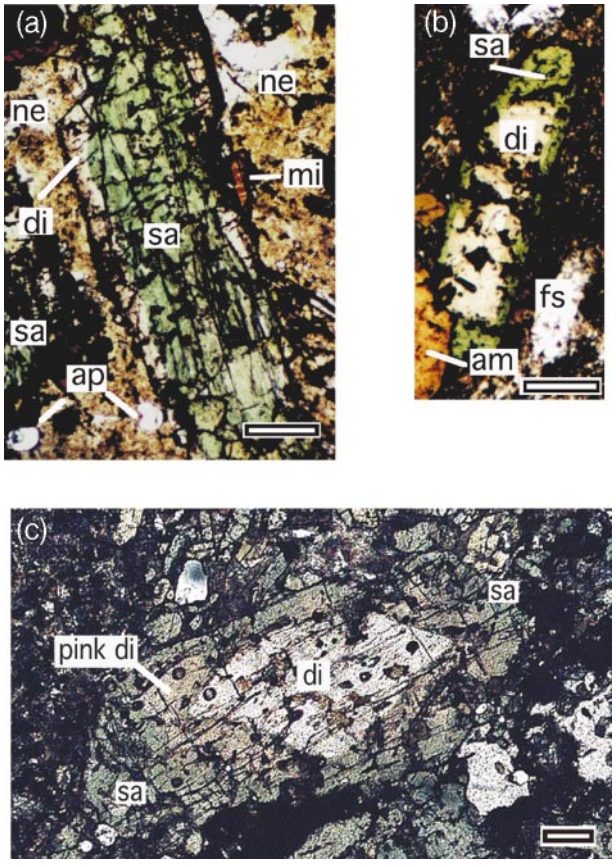


**Fig. 3.** Photomicrographs of clinopyroxenes from pyroxenites and host lamprophyres showing various styles of zoning: (a) sharp contact between a green salite core surrounded by colourless diopside rim continuously zoned to a pinkish diopside outer rim in pyroxenite THD; (b) colourless diopside core mantled by green salite in camptonite S6; (c) relict colourless diopside core mantled by pinkish diopside zoned to a green salite rim in pyroxenite TH4; the small brown circles correspond to ion beam spots. di, diopside; sa, salite; mi, mica; am, amphibole; fs, feldspar; ne, altered nepheline; ap, apatite. The scale bars represent 250 μm.

carbonate (sample ES7) or nearly pure albite $Ab_{97–99}$ (sample ES2), which may be the result of progressive fenitization. All these observations suggest that these rocks are not igneous carbonate-rich rocks, the so-called 'silico-carbonatites' of Le Maître *et al.* (1989), but are the result of sub-solidus metasomatic processes.

## Clinopyroxene chemistry and zoning

Diopside and/or salite are present in all the xenolith types and the host lamprophyres, and frequently exhibit complex zoning in pyroxenites and their host lamprophyres (Fig. 3). The zoning may be continuous or abrupt, normal or inverse (Fig. 4); for example: (1) colourless diopside cores are mantled by pinkish diopside or green salite, and green salitic cores are surrounded by colourless or pinkish diopside; (2) oscillatory zoning of diopsidic and salitic compositions occurs. The rounded cores are described as 'relict crystals'. Relict diopside crystals are also found in the kaersutitites, the alkali gabbros, the syenites and in the silicate parts of the carbonate-rich xenoliths.

Salite, which appears to have crystallized from more evolved magmas than the diopside as suggested by its lower mg-number (50–60 compared with 66–80), has lower $TiO_2$ (0·6–2 wt %) and $Al_2O_3$ (2–7 wt %) and higher $Na_2O$ (1·2–3·1 wt %) than diopside (6–11, 2·5–3 and 0·4–1·3 wt %, respectively) (Table 4, Fig. 4). Both salite and diopside are enriched in incompatible elements and exhibit identical primitive mantle normalized patterns in lamprophyres (Fig. 5a), and ultramafic and mafic xenoliths (Fig. 5b and c). In contrast, salite from nepheline syenite and the carbonate-rich xenoliths are characterized by more irregular trace element patterns including strong negative Ti and positive Zr (1983–8816 ppm) anomalies (Fig. 5d). A tendency for a negative Sr anomaly is evident in diopside (Fig. 5b), whereas salite shows no Sr anomaly (except the salite from gabbro S43) or a positive one, and a positive Zr anomaly (Fig. 5c). The REE are characterized by light REE (LREE) enrichment (chondrite-normalized values $La_N = 50–150$ and average $La_N/Yb_N = 8–16$). A slight negative Eu anomaly may be present in some salite. Salite usually shows slightly steeper LREE and middle REE (MREE) (La–Dy) profiles (average $Ce_N/Sm_N = 3·8$ compared with 2·2 in diopside) and has a flat Dy–Yb slope (average $Dy_N/Yb_N = 0·9$ compared with 2·7 in diopside) (Fig. 5).

The major and trace element compositions for salite and diopside are similar in the xenoliths and the host lamprophyres and show no systematic variation between cores and rims in individual pyroxene grains.

## The carbonate xenolith

A large (20 cm in diameter) carbonate-rich xenolith, composed almost entirely (90% by volume) of coarse-grained calcite, was collected from a camptonite dyke (sample 93.11) south of Djebel El Groun (Fig. 1b). The millimetre-sized crystals of calcite are commonly twinned and highly interlocking, which results in a granular texture (Fig. 2f). A few triple junctions at the grain margins have been observed. Non-carbonate constituents comprise rarely zoned millimetre- to micrometre-sized grains of pyrochlore, MnO-rich (2–3 wt %) salite, rounded apatite grains, magnetite, and rare celestine and hematite included in the calcite. Minor calcite also occurs as isolated rounded inclusions in apatite. In some parts of the carbonatite xenolith,

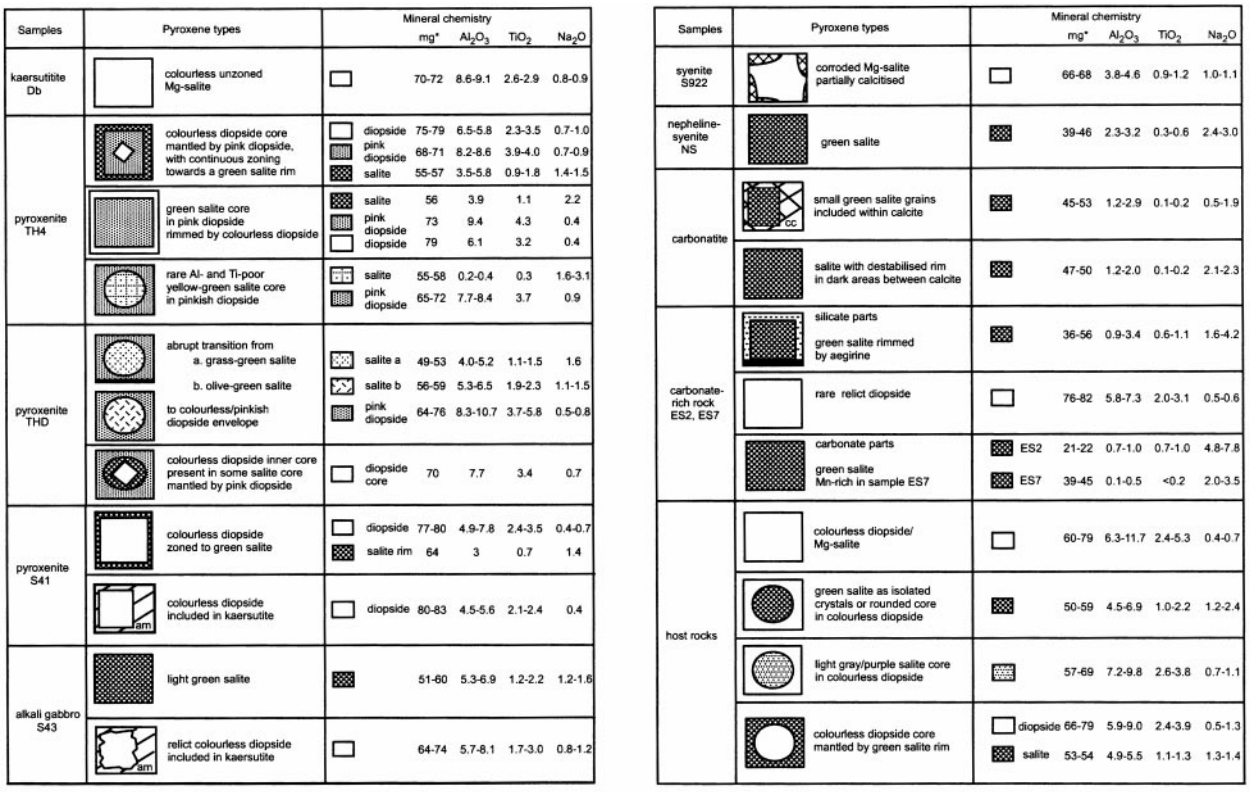


**Fig. 4.** Pyroxene assemblages in the various xenoliths and the host rocks. Abrupt and continuous zoning are respectively shown by concordant and discordant field limits. mg* (mg-number) = $100Mg/(Mg + Fe_{total})$; oxides in wt %; cc, calcite; am, amphibole.

a discrete, thin and dark vein network may be present between the calcite grains (Fig. 2f), or in rare interstitial patches that consist of a calcitized matrix with partially altered salite, zoned apatite, and magnetite inclusions. This irregular vein network may reflect late-stage fluid circulation. Data from a previous chemical and mineralogical study of this sample, including representative electron microprobe analyses by Mokhtari *et al.* (1996), are summarized in Table 5.

### *Carbonate*

Calcite is the only carbonate mineral observed and occurs as coarse grains or inclusions in apatite. The Taourirt calcite is Sr rich (2·5–2·8 wt % SrO, Table 5) and contains 0·5 wt % MnO, with low concentrations of BaO, FeO, MgO and REE.

### *Pyrochlore*

Pyrochlore ($Nb_2O_5$ 60–67 wt %) forms large (1 mm) zoned crystals and small unzoned grains included in calcite. The zoned crystals have a dark altered Ta- and U-rich (up to 1·7 and 5·2 oxide wt %, respectively) core (200 μm) rimmed by a colourless SrO-rich (up to 7·7 wt %) zone (100 μm) surrounded by a yellow CaO-rich (21 wt %) and low Sr, Ta and U marginal zone (300 μm) associated with an oxidized crystal rim (Table 5). Boundaries between the zones are sharp (Fig. 6), probably representing growth discontinuities. The small grains have a chemical composition similar to that of the yellow margin except for their higher MnO content (1·6–2·3 wt % compared with <0·4 wt %) (Mokhtari *et al.*, 1996). The REE patterns show positive Ce anomalies (Fig. 6).

### *Apatite*

Apatite forms two types of crystals: crystals up to 800 μm, which may be zoned and which show a thin outer rim in crossed nicols, and smaller (50 μm) frequently rounded crystals included in calcite crystals. The larger crystals are mostly prismatic; acicular crystals are rare. The prismatic crystals may include oval grains of anhedral calcite. Both types of apatite exhibit blue cathodoluminescence colours. They are Sr rich (1·0–1·7 SrO wt %) and F rich (up to 3·7 wt % F) with <0·1 oxide wt % of Mn, Si and Na, and low

*Table 4: Representative analyses of clinopyroxenes from the xenoliths and the host rock S6*

| | TH4 | | | THD | | S41 | Db | S43 | | S922 | NS | Carbonatite | | ES7 | Host rock S6 | | | |
|---|---|---|---|---|---|---|---|---|---|---|---|---|---|---|---|---|---|---|
| | Di* | Di | Sa | Sa*(og) | Sa*(gg) | Di* | Mg-Sa | Di* | Sa | Mg-Sa* | Sa | Sa[1] | Sa[11] | Sa | Sa* | Sa* | Sa* | Mg-Sa |
| $SiO_2$ | 46·32 | 44·31 | 49·67 | 46·70 | 46·60 | 48·34 | 46·09 | 48·89 | 46·12 | 49·33 | 50·53 | 49·55 | 50·19 | 51·04 | 47·49 | 47·10 | 47·46 | 45·37 |
| $Al_2O_3$ | 7·57 | 8·16 | 3·54 | 5·23 | 5·19 | 5·58 | 8·75 | 5·70 | 6·32 | 4·55 | 2·67 | 2·63 | 1·98 | 0·49 | 5·09 | 5·30 | 4·98 | 6·90 |
| $Cr_2O_3$ | 0·13 | 0·02 | 0·00 | 0·00 | 0·01 | 0·44 | 0·02 | 0·16 | 0·04 | 0·03 | 0·00 | 0·00 | 0·00 | 0·00 | 0·05 | 0·00 | 0·04 | 0·02 |
| $TiO_2$ | 2·79 | 3·98 | 0·92 | 1·93 | 1·51 | 2·42 | 2·78 | 1·66 | 2·02 | 1·18 | 0·34 | 0·16 | 0·18 | 0·17 | 1·28 | 1·30 | 1·12 | 2·39 |
| FeO | 6·23 | 7·92 | 12·43 | 11·84 | 13·30 | 5·05 | 7·72 | 7·62 | 12·81 | 10·60 | 15·26 | 12·89 | 14·38 | 16·63 | 13·13 | 13·68 | 12·95 | 10·63 |
| MgO | 12·12 | 10·76 | 9·30 | 9·70 | 8·58 | 13·67 | 10·98 | 12·05 | 8·57 | 10·99 | 7·21 | 8·25 | 7·93 | 5·99 | 8·49 | 8·30 | 8·79 | 9·50 |
| MnO | 0·09 | 0·13 | 0·30 | 0·28 | 0·42 | 0·05 | 0·04 | 0·14 | 0·37 | 0·37 | 0·72 | 2·44 | 1·95 | 3·07 | 0·46 | 0·46 | 0·46 | 0·35 |
| CaO | 23·25 | 23·22 | 21·61 | 22·00 | 21·31 | 23·45 | 22·00 | 23·36 | 21·47 | 21·31 | 18·86 | 21·66 | 19·55 | 17·12 | 20·97 | 21·04 | 20·94 | 21·49 |
| $Na_2O$ | 0·67 | 0·74 | 1·52 | 1·08 | 1·56 | 0·36 | 0·83 | 0·78 | 1·54 | 1·19 | 2·72 | 1·51 | 2·22 | 3·54 | 1·65 | 1·63 | 1·61 | 1·21 |
| $Fe_2O_3$† | 3·25 | 4·28 | 4·25 | 5·59 | 7·19 | 1·36 | 1·95 | 3·15 | 6·83 | 3·71 | 5·43 | 6·03 | 6·29 | 8·43 | 5·90 | 6·63 | 6·25 | 5·18 |
| FeO | 3·31 | 4·07 | 8·60 | 6·81 | 6·83 | 3·83 | 5·96 | 4·79 | 6·67 | 7·26 | 10·37 | 7·46 | 8·73 | 9·05 | 7·82 | 7·71 | 7·33 | 5·97 |
| Total | 99·50 | 99·67 | 99·71 | 99·32 | 99·20 | 99·50 | 99·40 | 100·66 | 99·96 | 99·91 | 98·87 | 99·69 | 99·02 | 98·90 | 99·20 | 99·47 | 98·98 | 98·3 |
| mg-no. | 77·6 | 70·8 | 57·1 | 59·3 | 53·5 | 82·8 | 71·7 | 73·8 | 54·4 | 64·9 | 45·7 | 53·3 | 49·6 | 39·1 | 53·5 | 51·9 | 54·7 | 61·4 |
| Wo | 48·7 | 49·5 | 49·5 | 48·8 | 49·7 | 47·7 | 46·4 | 49·0 | 49·3 | 46·6 | 48·9 | 50·4 | 48·4 | 48·8 | 49·0 | 49·0 | 48·7 | 48·3 |
| En | 44·5 | 41·6 | 33·1 | 36·8 | 34·8 | 45·2 | 41·4 | 41·6 | 35·2 | 38·9 | 28·2 | 32·9 | 31·9 | 27·7 | 33·6 | 33·4 | 34·9 | 38·3 |
| Fs | 6·8 | 8·9 | 17·3 | 14·4 | 15·5 | 7·2 | 12·5 | 9·4 | 15·5 | 14·5 | 22·9 | 16·7 | 19·7 | 23·5 | 17·4 | 17·5 | 16·4 | 13·6 |
| Sc | 57·1 | 37·5 | 50·7 | 40·1 | 40·6 | 93 | | 105 | 35·4 | 77·3 | 42·1 | 59·6 | 31·8 | 158 | 50·6 | 62·9 | 41·5 | 48·8 |
| V | 272 | 270 | 379 | 344 | 339 | 370 | | 306 | 315 | 189 | 471 | 979 | 920 | 666 | 319 | 297 | 303 | 259 |
| Sr | 306 | 740 | 1105 | 1752 | 1546 | 277 | | 156 | 342 | 157 | 197 | 2279 | 733 | 385 | 233 | 216 | 267 | 428 |

*Table 4: continued*

| | TH4 | | | THD | | S41 Db | | S43 | | S922 | NS | Carbonatite | | ES7 | Host rock S6 | | | |
|---|---|---|---|---|---|---|---|---|---|---|---|---|---|---|---|---|---|---|
| | Di* | Di | Sa | Sa*(og) | Sa*(gg) | Di* | Mg-Sa | Di* | Sa | Mg-Sa* | Sa | Sa[1] | Sa[11] | Sa | Sa* | Sa* | Sa* | Mg-Sa |
| Y | 16·3 | 32·8 | 11·3 | 8·8 | 14 | 30·9 | | 9·5 | 27·5 | 67·4 | 23·1 | 39·1 | 14·6 | 55·8 | 9·2 | 8·9 | 13·7 | 26·7 |
| Zr | 148 | 592 | 541 | 464 | 542 | 231 | | 120 | 581 | 300 | 1983 | 617 | 601 | 8816 | 589 | 629 | 631 | 420 |
| Ba | 0·69 | 0·54 | 2·2 | 0·20 | 0·28 | 0·38 | | 7·0 | 4·2 | 0·23 | 1·04 | 50·6 | 1·4 | 9·3 | 5·9 | 0·36 | 0·26 | 0·56 |
| La | 14·6 | 43·8 | 21·6 | 20·1 | 28·8 | 27·1 | | 20·6 | 42·5 | 57·8 | 80·6 | 85·5 | 65·9 | 37·3 | 17·9 | 15·5 | 27·0 | 33·5 |
| Ce | 60·7 | 168 | 61·9 | 55·0 | 91·4 | 89·3 | | 62·0 | 153 | 218 | 203 | 254 | 171 | 142 | 45·2 | 44·2 | 65·8 | 121 |
| Nd | 32·5 | 90·5 | 21·9 | 15·9 | 29·3 | 44·7 | | 22·9 | 68·3 | 109 | 59·2 | 92·9 | 54·1 | 53·6 | 13·8 | 13·1 | 18·5 | 47·4 |
| Sm | 7·2 | 17·2 | 4·2 | 3·0 | 5·5 | 12·6 | | 6·0 | 12·4 | 24·6 | 9·2 | 18·4 | 8·3 | 13·6 | 2·8 | 2·6 | 3·9 | 10·4 |
| Eu | 1·6 | 3·3 | 1·2 | 0·31 | 1·1 | 3·0 | | 1·6 | 2·7 | 3·1 | 2·7 | 2·5 | 0·87 | 2·3 | 0·44 | 0·58 | 0·53 | 2·4 |
| Gd | 5·2 | 9·2 | 3·7 | 1·9 | 2·9 | 9·1 | | 3·9 | 10·2 | 14·5 | 2·7 | 10·6 | 7·4 | 9·3 | 2·0 | 2·6 | 2·7 | 6·5 |
| Dy | 3·8 | 6·6 | 2·1 | 1·5 | 2·2 | 6·1 | | 2·5 | 5·9 | 15·1 | 3·2 | 7·4 | 3·8 | 9·6 | 1·6 | 1·5 | 1·9 | 5·3 |
| Er | 1·6 | 2·9 | 1·02 | 1·06 | 1·5 | 2·4 | | 1·02 | 3·0 | 7·5 | 13·5 | 4·0 | 1·9 | 8·9 | 1·1 | 1·1 | 1·2 | 2·6 |
| Yb | 0·73 | 1·8 | 1·2 | 1·2 | 1·5 | 0·99 | | 0·83 | 2·4 | 4·6 | 7·2 | 3·8 | 1·6 | 19·3 | 1·3 | 1·2 | 1·3 | 1·7 |

Pyroxenites: TH4, THD, S41. Kaersutitite: Db. Alkali gabbro: S43. Syenite: S922. Nepheline syenite: NS. Carbonate-rich rock: ES7: Carbonatite: 1 and 11: salite included or between calcite grains. Di, diopside; Sa, salite; Mg-Sa, Mg salite; og, olive green; gg, grass green. mg-no. $= 100\,Mg/(Mg + Fe_{total})$. Analytical methods: electron microprobe analysis (EMPA) for major elements (oxide weight %) and ion microprobe (secondary ionization mass spectrometry) for trace elements (ppm). No trace element data available for Db.

*Relict phase.

†Calculated.

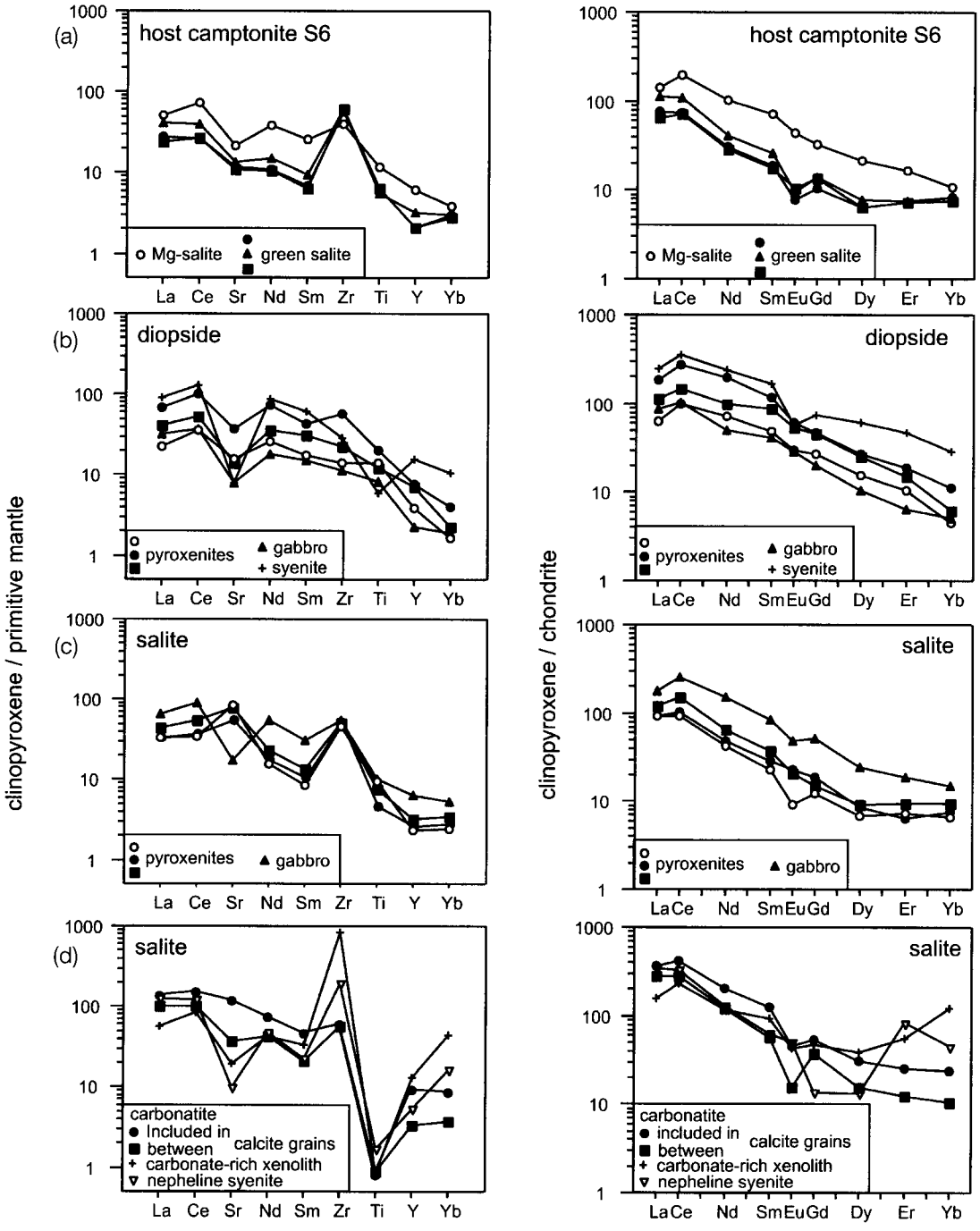


**Fig. 5.** Primitive mantle normalized trace element and chondrite-normalized REE plots for clinopyroxenes from selected rocks: (a) clinopyroxenes from host camptonite S6; (b) diopside in xenoliths, (c) and (d) salite in xenoliths. Clinopyroxenes analyses are given in Table 4. Normalization constants from McDonough & Sun (1995).

$\sum$LREE (<0·7 oxide wt %) (Table 5). The large zoned crystals show sharp boundaries between $SiO_2$- and LREE-rich rims, and $P_2O_5$-, SrO- and F-rich cores (Fig. 7a). Both types of apatite have low La contents (<1500 ppm) and $\sum$LREE, and rather flat LREE patterns (Fig. 7b) with $(La/Nd)_N$ of 1·3 (coarse apatite) to 2·5 (apatite inclusion). In detail, the shape of the LREE pattern differs between the coarse grains and

*Table 5: Electron microprobe analyses of carbonatite minerals*

| | Cc | Py c | Py r | Py m | Ap inc | Ap cg |
|---|---|---|---|---|---|---|
| FeO | 0·01 | 2·43 | 2·86 | 1·67 | 0·08 | 0·10 |
| MnO | 0·46 | 0·36 | 0·03 | 0·48 | 0·09 | 0·09 |
| MgO | 0·08 | | | | | |
| CaO | 53·60 | 12·69 | 8·56 | 20·72 | 54·10 | 53·90 |
| SrO | 2·74 | 0·82 | 7·40 | 0·37 | 1·66 | 1·60 |
| $Na_2O$ | 0·02 | 3·32 | 0·81 | 3·07 | 0·16 | 0·14 |
| BaO | 0·08 | | | | | |
| $SiO_2$ | | | | | 0·03 | 0·01 |
| $Al_2O_3$ | | | | | | |
| $TiO_2$ | | 3·25 | 2·83 | 2·51 | | |
| F | | 0·01 | 0·02 | 0·02 | 3·58 | 3·62 |
| Cl | | | | | 0·05 | 0·08 |
| $P_2O_5$ | | | | | 40·97 | 41·42 |
| $La_2O_3$ | 0·11 | 0·25 | 0·50 | 0·28 | 0·19 | 0·21 |
| $Ce_2O_3$ | 0·17 | 1·29 | 1·97 | 1·45 | 0·28 | 0·24 |
| $Nd_2O_3$ | | 0·38 | 0·38 | 0·52 | 0·15 | 0·17 |
| $Nb_2O^+$ | | 64·29 | 67·34 | 67·03 | | |
| $Ta_2O_5$ | | 1·71 | 0·58 | 0·06 | | |
| $ZrO_2$ | | 0·07 | 0·16 | 0·16 | | |
| $UO_2$ | | 4·60 | 1·08 | 0·02 | | |
| $ThO_2$ | | 0·12 | 0·09 | 0·06 | | |
| Total | 57·27 | 95·59 | 94·61 | 98·42 | 99·82 | 100·04 |

Cc, calcite; Py, pyrochlore; Ap, apatite; c, dark core; r, thin colourless rim; m, yellow margin; inc, inclusion; cg, coarse grain. FeO = total iron. Total minus F, Cl = O.

the inclusions of apatite, as the LREE pattern of the former shows a negative Ce anomaly.

*Pyroxene*

Pyroxenes, either included in calcite or in the dark veins and patches, are MnO-rich (2–3 wt %), $TiO_2$-poor (<0·2 wt %) salite (Fig. 4). $Na_2O$ and $Al_2O_3$ contents (1·2–2·9 and 0·5–1·9 wt %, respectively), and mg-number values (45–53) are variable. The salite is rich in Sr, up to 0·23 wt % in grains included in calcite, and highly LREE enriched (chondrite-normalized values $La_N$ = 199–262 and $La_N/Yb_N$ = 15–27; Table 4).

## BULK-ROCK CHEMISTRY

The major and trace element compositions of the carbonatite and silicate rocks are given in Table 6. These include eight xenoliths and six host camptonites and monchiquites from the Teniet El Amra and Djebel El Groun outcrops, and two samples from the eastern part of the Taourirt area, monchiquite MJ1 and olivine nephelinite CH31. Additional analyses of lamprophyre and nephelinite, which have been previously published by Giret (1985), Mokhtari & Velde (1988) and Wagner *et al.* (1996), are not included in Table 6 but are included for comparison in Fig. 8.

### Alkaline lamprophyres

For all bulk chemical analyses the loss on ignition values (representing $H_2O$ as well as $CO_2$) vary from 2% to almost 9%, indicating significant alteration products. Taking into account the variations that could result from secondary alteration, the rocks appear strongly undersaturated with respect to silica as demonstrated by the presence of nepheline, leucite and even larnite in the CIPW norm for some samples. MgO and CaO contents show strong variations (2·2–16 and 5·8–14·9 wt %, respectively). The monchiquite S5 has high MgO and CaO abundances (16 and 12·67 wt %, respectively) and is picritic, rich in cumulate olivine and clinopyroxene.

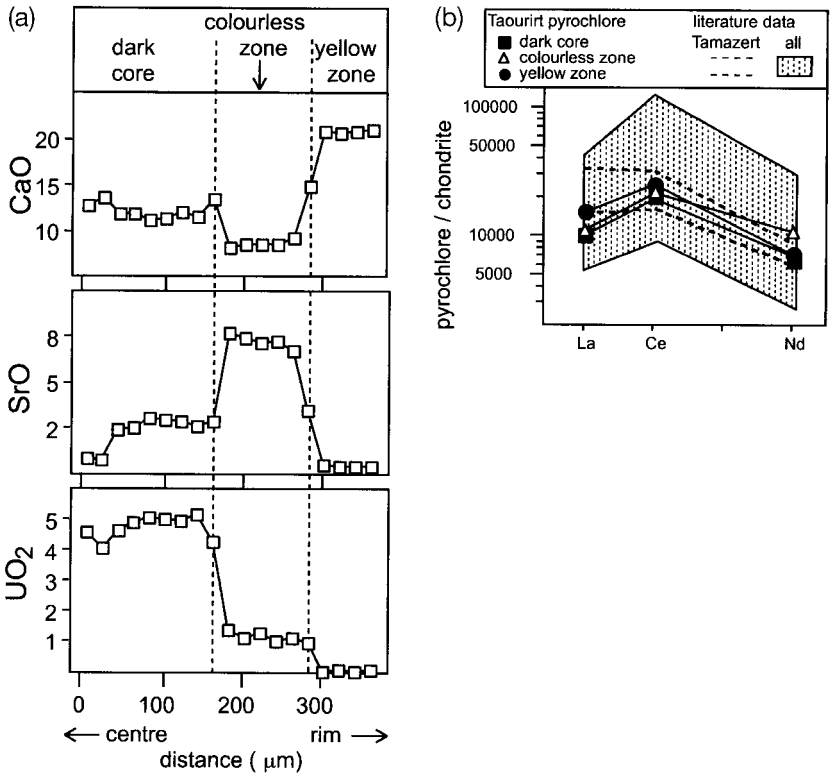


**Fig. 6.** Carbonatite pyrochlore characteristics. (a) Compositional profiles from core to rim in a zoned crystal; one analytical point every 20 μm; oxides in wt %. Representative analyses of each zone are given in Table 5. (b) Chondrite-normalized patterns for LREE. Each point corresponds to an average value. Normalization values as in Fig. 5. Data from the literature (shaded field): Blackburn (Hogarth *et al.*, 1988); Kaiserstuhl, Oka, Fen and Sökli (Hornig-Kjarsgaard, 1998); the dashed lines delimit the range of composition of pyrochlore from Tamazert (Mourtada, 1997).

The compositions of the Taourirt rocks are similar to global average compositions of camptonites and monchiquites (Rock, 1991). Figure 8 shows the variations of several major element oxides vs MgO and some trace elements vs Th for the host lamprophyres, compared with data for other alkaline rocks from different outcrops in the Taourirt area. Contents of compatible trace elements (e.g. Ni and Cr) define a considerable range from 17 to 218 ppm and 3·9 to 448 ppm, respectively. The more primitive lamprophyres contain >200 ppm Ni and Cr, with even higher contents in the cumulate rock S5 (Table 6). The rocks have variable but high abundances in Sr (100–2360 ppm), Rb (24–144 ppm) and Ba (970–1428 ppm), which may reflect the presence of plagioclase, K-feldspar and biotite. Linear trends (Fig. 8) are observed for most major ($Al_2O_3$, alkalis, CaO and $TiO_2$) and some trace elements (e.g. Ni, Cr, Zr, U and Th) from primitive monchiquites (high mg-number = 66) towards more evolved rocks (mg-number = 30), as illustrated in Fig. 8. Other elements such as Rb and Ba exhibit no systematic variation with differentiation (e.g. Rb plot in Fig. 8).

Primitive mantle normalized trace element patterns are characterized by a general decrease in abundance from Rb to heavy REE (HREE), and show negative anomalies in K, P and Sm relative to the adjacent elements (Fig. 9a). All the samples show subparallel LREE-enriched profiles with a steep gradient [$La_N$ = 163–262, $(La/Yb)_N$ = 25–36, Table 6], typical of undersaturated alkaline rocks, and lack Eu anomalies. Their trace element contents fall within the range of the abundances reported in other lamprophyres from Taourirt (Mokhtari & Velde, 1988; Mokhtari, 1995) and in the alkaline lamprophyres from the Tamazert complex (Bouabdli *et al.*, 1988; Bouabdli, 1993) (Fig. 9).

## Olivine nephelinites

Their composition is not unlike that of the most primitive lamprophyres, as they are rich in MgO and CaO (~12 wt %) and have high mg-number (68), and Ni and Cr contents (251 and 265 ppm, respectively) (Fig. 8). The trace element contents are similar to those of the lamprophyres (Fig. 9a).

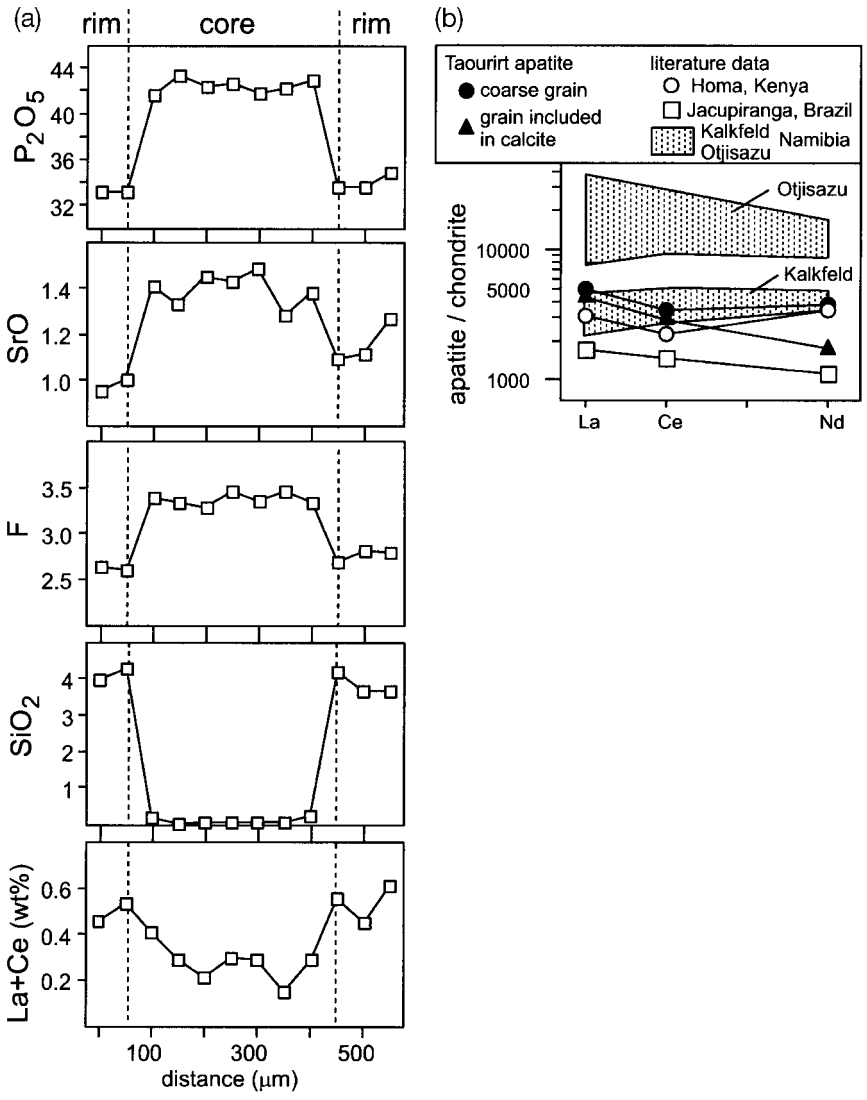


**Fig. 7.** Carbonatite apatite characteristics. (a) Traverse across a large (700 μm width) zoned apatite; one analytical point every 50 μm; oxides and REE in wt %. (b) LREE distribution in apatites from Taourirt compared with magmatic apatites (average values) from various carbonatite occurrences taken from Hornig-Kjarsgaard (1998) and Bühn *et al.* (2001). Normalization constants as in Fig. 5.

## Alkaline silicate xenoliths

### *Pyroxenites and kaersutitites*

Petrographic examination of thin sections of some samples (e.g. pyroxenite THC and kaersutitite Db) clearly indicates their cumulative nature, whereas in the other samples the extent of accumulation is difficult to ascertain and thus the degree to which these rocks approximate magma compositions is difficult to evaluate. The major element composition of the pyroxenites is similar to that of the intrusive pyroxenites ('melanocratic mestigmerites') described by Giret (1985), except for lower alkali contents (Fig. 8). One may argue, therefore, that the chemical composition for some Taourirt xenoliths represents that of a melt. However, this hypothesis cannot be verified completely because trace element data are lacking for the intrusive pyroxenites (Giret, 1985).

The two pyroxenites (THD, THC) have similar compositions (Table 6) and sample THD is typically silica undersaturated, with olivine and nepheline in the CIPW norm. Their primitive mantle normalized trace element patterns are enriched in incompatible elements (60–100 times the primitive mantle) and are relatively depleted in the least incompatible elements (Fig. 9c). The chondrite-normalized REE profiles are parallel, enriched in LREE (300–600 times the

*Table 6: Major and trace element data for Taourirt rocks*

| | Carbonatite | Krs | Pyroxenites | | Gabbros | | | Ne-syen | Cxeno | Host rocks | | | | | | Mon | Ol-neph |
|---|---|---|---|---|---|---|---|---|---|---|---|---|---|---|---|---|---|
| | 923 | Db | THD | THC | Scn | Scb | S43 | NS | ES2 | S2 | S3 | S4 | S5 | S6 | 93·11 | MJ1 | CH31 |
| *Major elements (wt %)* | | | | | | | | | | | | | | | | | |
| $SiO_2$ | 3·10 | 37·62 | 35·12 | 33·83 | 38·71 | 42·75 | 43·45 | 50·87 | 55·81 | 42·13 | 42·96 | 49·17 | 38·87 | 49·54 | 43·95 | 35·75 | 40·84 |
| $Al_2O_3$ | 0·48 | 12·84 | 13·12 | 11·78 | 14·95 | 17·73 | 15·57 | 21·50 | 15·96 | 15·06 | 15·01 | 17·74 | 9·41 | 17·93 | 16·80 | 10·91 | 12·85 |
| $Fe_2O_3^*$ | 3·37 | 14·11 | 8·65 | 17·75 | 14·38 | 12·16 | 12·11 | 2·82 | 2·68 | 5·68 | 5·78 | 2·12 | 11·24 | 3·67 | 3·85 | 8·06 | 4·23 |
| FeO | | | 5·41 | | | | | | | 5·08 | 5·16 | 4·15 | | 2·71 | 4·37 | 4·92 | 6·53 |
| MnO | 0·43 | 0·11 | 0·20 | 0·26 | 0·24 | 0·18 | 0·20 | 0·09 | 0·15 | 0·15 | 0·14 | 0·17 | 0·16 | 0·16 | 0·14 | 0·17 | 0·17 |
| MgO | 0·36 | 12·49 | 7·63 | 7·29 | 7·97 | 5·66 | 4·30 | 1·24 | 0·20 | 6·83 | 7·53 | 2·43 | 16·00 | 2·22 | 3·80 | 10·67 | 12·36 |
| CaO | 50·64 | 12·35 | 13·09 | 13·57 | 10·00 | 8·91 | 9·16 | 3·96 | 8·25 | 11·24 | 10·35 | 5·83 | 12·67 | 5·94 | 7·53 | 15·68 | 12·4 |
| $Na_2O$ | 0·04 | 1·63 | 2·65 | 2·72 | 2·57 | 3·45 | 3·76 | 6·50 | 9·71 | 3·81 | 2·70 | 6·23 | 1·54 | 5·49 | 4·40 | 1·28 | 3·7 |
| $K_2O$ | 0·04 | 1·87 | 1·83 | 1·22 | 2·66 | 2·53 | 2·43 | 4·51 | 0·12 | 2·49 | 2·86 | 4·71 | 0·93 | 4·57 | 4·18 | 1·39 | 1·17 |
| $TiO_2$ | 0·06 | 4·77 | 3·99 | 4·74 | 4·13 | 3·22 | 3·53 | 0·37 | 0·51 | 4·09 | 4·01 | 1·92 | 2·65 | 1·79 | 2·72 | 3·80 | 3·2 |
| $P_2O_5$ | 0·37 | 0·05 | 1·63 | 2·05 | 0·83 | 0·61 | 0·88 | 0·10 | 0·04 | 0·67 | 0·65 | 0·37 | 0·56 | 0·35 | 0·49 | 1·10 | 0·57 |
| LOI | 39·19 | 1·12 | 4·91 | 4·33 | 2·36 | 2·61 | 3·57 | 6·81 | 6·84 | 3·32 | 3·41 | 3·38 | 4·50 | 4·08 | 6·60 | 6·83 | 1·96 |
| Total | 98·07 | 98·95 | 98·23 | 99·54 | 98·80 | 99·81 | 98·96 | 98·77 | 100·27 | 100·55 | 100·56 | 98·22 | 98·53 | 98·45 | 98·83 | 100·56 | 99·98 |
| mg-no. | 17·5 | 63·7 | 50·4 | 44·8 | 52·3 | 48·0 | 41·3 | 46·5 | 12·9 | 54·4 | 56·4 | 41·1 | 73·8 | 39·8 | 46·4 | 60·9 | 68·1 |
| *Trace elements (ppm)* | | | | | | | | | | | | | | | | | |
| Sc | 0·02 | 24·5 | 14·4 | 11·8 | 30·1 | 24·2 | 9·7 | 0·91 | 0·35 | | | 5·8 | 23 | 4·9 | 10·3 | | |
| V | 151 | 340 | 290 | 365 | 263 | 213 | 211 | 34 | 63·1 | | | 128 | 204 | 122 | 197 | | 306 |
| Cr | 0·8 | 3·6 | | | 122 | 100 | | | 0·6 | | | 6·3 | 445 | 3·9 | tr | | 265 |
| Co | 2·4 | 64 | 46 | 67 | 47 | 40 | 29 | 6·6 | 3·2 | | | 19·1 | 61 | 16·5 | 22·2 | | 63 |
| Ni | 0·6 | 79 | 27 | 30 | 72 | 63 | 19 | 6·8 | 1·6 | | | 21 | 314 | 17 | 18·6 | | 251 |
| Cu | 17 | 65 | 92 | 116 | 81 | 78 | 39 | 8 | 21 | | | 44 | 44 | 38 | 48 | | 57 |
| Zn | 8·3 | 89 | 164 | 201 | 150 | 134 | 195 | 69 | 107 | | | 126 | 97 | 120 | 148 | | 91 |
| Nb | 255 | 18 | 58 | 132 | 55 | 48 | 139 | 40 | 100 | 112 | 102 | 156 | 90 | 144 | 112·5 | 133 | 95 |
| Rb | 0·73 | 14·95 | 62·55 | 30·09 | 72·21 | 70·42 | 34·62 | 89·25 | 1·8 | 47 | 64 | 144 | 30 | 131 | 98·3 | 40·8 | 27·55 |

*Table 6: continued*

| | Carbonatite | Krs | Pyroxenites | | Gabbros | | | Ne-syen | Cxeno | Host rocks | | | | | | Mon | Ol-neph |
|---|---|---|---|---|---|---|---|---|---|---|---|---|---|---|---|---|---|
| | 923 | Db | THD | THC | Scn | Scb | S43 | NS | ES2 | S2 | S3 | S4 | S5 | S6 | 93·11 | MJ1 | CH31 |
| *Trace elements (ppm)* | | | | | | | | | | | | | | | | | |
| Sr | 14300 | 706 | 1791 | 1846 | 1350 | 1949 | 2369 | 1943 | 645 | 2364 | 1105 | 1803 | 1363 | 1573 | 1107 | 1570 | 1214 |
| Zr | 38 | 106 | 267 | 320 | 185 | 141 | 298 | 170 | 180 | 285 | 273 | 517 | 240 | 500 | 319 | 383 | 251 |
| Hf | 0·87 | | | | | | | | | 5·8 | 5·74 | 8·54 | 5·03 | 8·07 | 6·15 | 7·96 | |
| Y | 90·7 | 12·6 | 31 | 40 | 39 | 30·8 | 41·5 | 8·8 | 8·4 | | | 20·2 | 18·1 | 19·5 | 22·8 | 33·8 | 19·2 |
| Ba | 411 | 1403 | 1594 | 451 | 1220 | 1278 | 1332 | 1103 | 611 | 1150 | 1036 | 1288 | 618 | 1080 | 1428 | 1254 | 906 |
| Th | 1·14 | 0·35 | 5·81 | 22·5 | 4·27 | 3·95 | 10·81 | 7·87 | 10·4 | 7·13 | 6·69 | 17·88 | 6·79 | 17·10 | 9·10 | 12·13 | 7·98 |
| U | 9·72 | 0·2 | 2·68 | 6·51 | 1·15 | 1·85 | 2·39 | 2·48 | 5·05 | 2·39 | 2·12 | 5·62 | 2·38 | 5·48 | 3·32 | 3·7 | 2·06 |
| *Rare earth elements (ppm)* | | | | | | | | | | | | | | | | | |
| La | 321 | 9 | 99 | 181 | 88 | 72 | 173 | 57 | 16 | 60·5 | 53·5 | 86·27 | 65·07 | 79·87 | 75·89 | 96·14 | 62 |
| Ce | 637 | 29 | 200 | 383 | 188 | 151 | 339 | 77 | 35 | 119·73 | 106·36 | 148·52 | 128·27 | 135·8 | 139 | 189·66 | 123 |
| Pr | 69·4 | 4·78 | 22·8 | 42·18 | 22·5 | 17·9 | 34·8 | 6·11 | 3·88 | 13·6 | 12·24 | 14·99 | 14·55 | 13·55 | 14·44 | 21·84 | 13·96 |
| Nd | 245 | 24·5 | 87·4 | 153·7 | 88·3 | 69·8 | 119 | 17·6 | 14 | 53·3 | 48·62 | 52·15 | 55·76 | 46·81 | 53·22 | 84·11 | 52 |
| Sm | 38·2 | 6·04 | 14·7 | 23·8 | 16·1 | 12·6 | 17·8 | 2·35 | 2·39 | 9·46 | 8·89 | 8·11 | 9·23 | 7·24 | 9·07 | 14·12 | 8·9 |
| Eu | 11·9 | 2·21 | 4·71 | 7 | 4·47 | 3·58 | 5·18 | 0·823 | 0·875 | 2·96 | 2·83 | 2·45 | 2·83 | 2·18 | 2·9 | 4·11 | 2·77 |
| Gd | 30 | 4·79 | 11·5 | 17·8 | 12·4 | 9·69 | 13·8 | 2·17 | 1·87 | 8·15 | 7·78 | 6·74 | 7·55 | 5·95 | 7·22 | 11·46 | 6·84 |
| Tb | 3·91 | 0·66 | 1·47 | 2·15 | 1·71 | 1·32 | 1·78 | 0·267 | 0·285 | 1·12 | 1·06 | 0·97 | 1·04 | 0·86 | 0·96 | 1·6 | 0·884 |
| Dy | 18·5 | 3·23 | 6·95 | 9·608 | 8·59 | 6·82 | 8·92 | 1·452 | 1·58 | 5·33 | 5·12 | 4·69 | 4·78 | 4·18 | 4·85 | 7·56 | 4·28 |
| Ho | 3·13 | 0·497 | 1·17 | 1·58 | 1·52 | 1·2 | 1·58 | 0·277 | 0·303 | 0·9 | 0·85 | 0·83 | 0·78 | 0·74 | 0·88 | 1·25 | 0·731 |
| Er | 7·22 | 1 | 2·64 | 3·48 | 3·56 | 2·84 | 3·89 | 0·745 | 0·782 | 2·09 | 1·99 | 2·1 | 1·80 | 1·91 | 2·03 | 2·97 | 1·67 |
| Tm | 0·96 | 0·115 | 0·343 | 0·438 | 0·501 | 0·396 | 0·573 | 0·123 | 0·132 | 0·26 | 0·25 | 0·29 | 0·22 | 0·26 | 0·28 | 0·36 | 0·224 |
| Yb | 5 | 0·541 | 1·76 | 2·18 | 2·66 | 2·1 | 3·02 | 0·794 | 0·722 | 1·54 | 1·45 | 1·85 | 1·27 | 1·64 | 1·68 | 2·17 | 1·16 |
| Lu | 0·633 | 0·072 | 0·236 | 0·285 | 0·362 | 0·29 | 0·412 | 0·124 | 0·097 | 0·22 | 0·21 | 0·29 | 0·18 | 0·25 | 0·235 | 0·31 | 0·158 |

mg-no. $= 100Mg/(Mg + Fe_{total})$. Analytical methods: see text. tr, trace; Krs, kaersutitite; Ne-syen, nepheline syenite; Cxeno, carbonate-rich xenolith; Mon, monchiquite; Ol-neph, olivine nephelinite.
*Total iron expressed as $Fe_2O_3$ for samples where FeO is not reported.

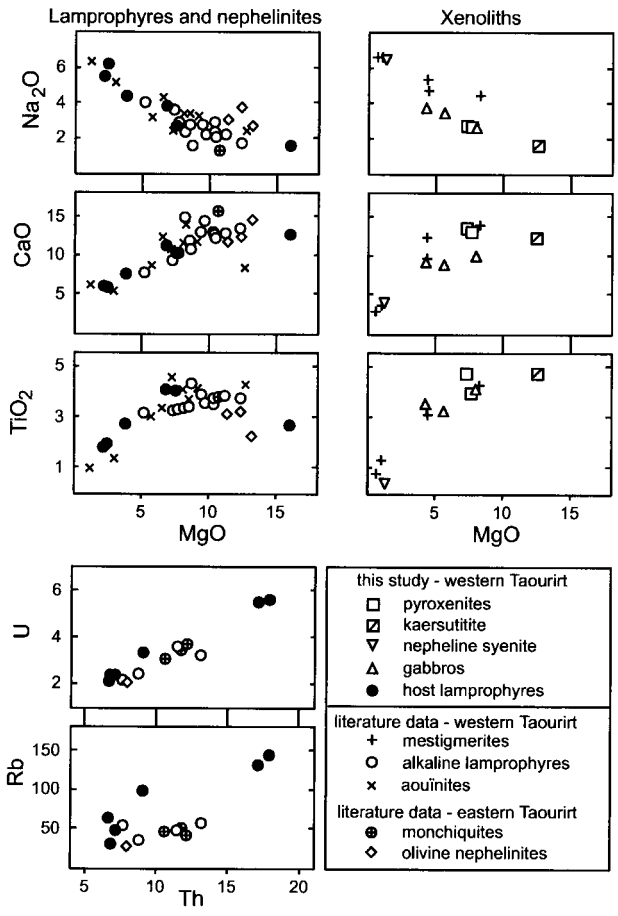


**Fig. 8.** Whole-rock variation diagrams of some major and trace element abundances (in wt % and ppm, respectively) for lamprophyres and silicate xenoliths from Teniet El Amra and Djebel El Groun (this study) compared with alkaline rocks from various outcrops of the Taourirt area (Giret, 1985; Mokhtari & Velde, 1988; Mokhtari, 1995; Wagner *et al.*, 1996). Literature data: mestigmerites, alkaline lamprophyres and aouïnites from Teniet El Amra, Djebel El Groun, Ferme Dubois and Krandbaa (western Taourirt); monchiquites from Koudiat Moujniba and olivine nephelinites from Koudiat Chmedda (eastern Taourirt). (See Fig. 1b for the location of the outcrops.)

chondrites), and steep [$(La/Yb)_N$ = 37–55; Fig. 9d]. The high contents of Th, U and LREE in sample THC may indicate the presence of cumulative titanite (Table 6). The normalized trace element pattern of the kaersutitite Db shows strong negative Th and P anomalies (Fig. 9c), and an REE profile less enriched [$(La/Yb)_N$ = 11] and convex upward compared with those of the pyroxenites (Fig. 9d). Both features may be attributed to the abundance of amphibole, and the cumulate nature of the kaersutitite is reflected in its distinctly high Sc/Yb ratio.

*Amphibole-bearing alkali gabbros*

Two samples (Sc, S43) were selected based on their modal compositions (Table 3), with mg-number that ranges between 48 and 41 and similar total alkali contents (~6·3 wt %). Sample Sc is mineralogically heterogeneous, which is mainly reflected in the higher mg-number (48) and lower silica content of the more melanocratic part (Scn, Table 6). All gabbro samples are enriched in incompatible elements, with the highest content in the most differentiated sample (sample S43, Table 6). Their trace element normalized patterns are similar to those of the pyroxenites (Fig. 9c).

*Nepheline syenite*

The nepheline syenite NS is not peralkaline [peralkalinity index, PI = mol$(Na_2O + K_2O)/Al_2O_3 < 1$], its combined concentration of Sr + Ba (3016 ppm) and its low Zr (170 ppm) content are not comparable with those of 'agpaitic' nepheline syenites from complexes of similar nature (Edgar, 1974). Its major element composition is not unlike that of the intrusive samples reported by Giret (1985) from the same area, except for lower $TiO_2$ and CaO contents, and higher $Al_2O_3/TiO_2$ ratio (Table 6, Fig. 8).

The primitive mantle normalized trace element pattern is similar to that of the pyroxenites with 100–250 times the primitive mantle abundances from Rb to Sr, but exhibits lower abundances for more compatible elements (from P to Lu) and strong negative P and Sm anomalies (Fig. 9c). The nepheline syenite has lower overall REE abundances compared with the pyroxenites, and exhibits a different concave-up REE pattern with a steeper LREE part [$(La/Sm)_N$ = 15 compared with 4–5 in pyroxenites] (Fig. 9d). The trace element profile resembles that of nepheline syenites from the Tamazert alkaline complex (Bouabdli, 1993) (Fig. 9e).

*Carbonate-rich xenoliths*

The primitive mantle normalized pattern of sample ES2 shows an extremely irregular profile for the most incompatible elements with strong negative K and P anomalies, as observed in the carbonate xenolith, but a smoother profile for the most compatible elements not unlike that of the nepheline syenite (Fig. 9c). The overall REE abundances are lower than those of the other rocks, except the nepheline syenite. The chondrite-normalized REE pattern resembles that of the nepheline syenite, except for lower LREE enrichment ($La_N$ = 49 compared with 200 times chondritic in the nepheline syenite; Fig. 9d).

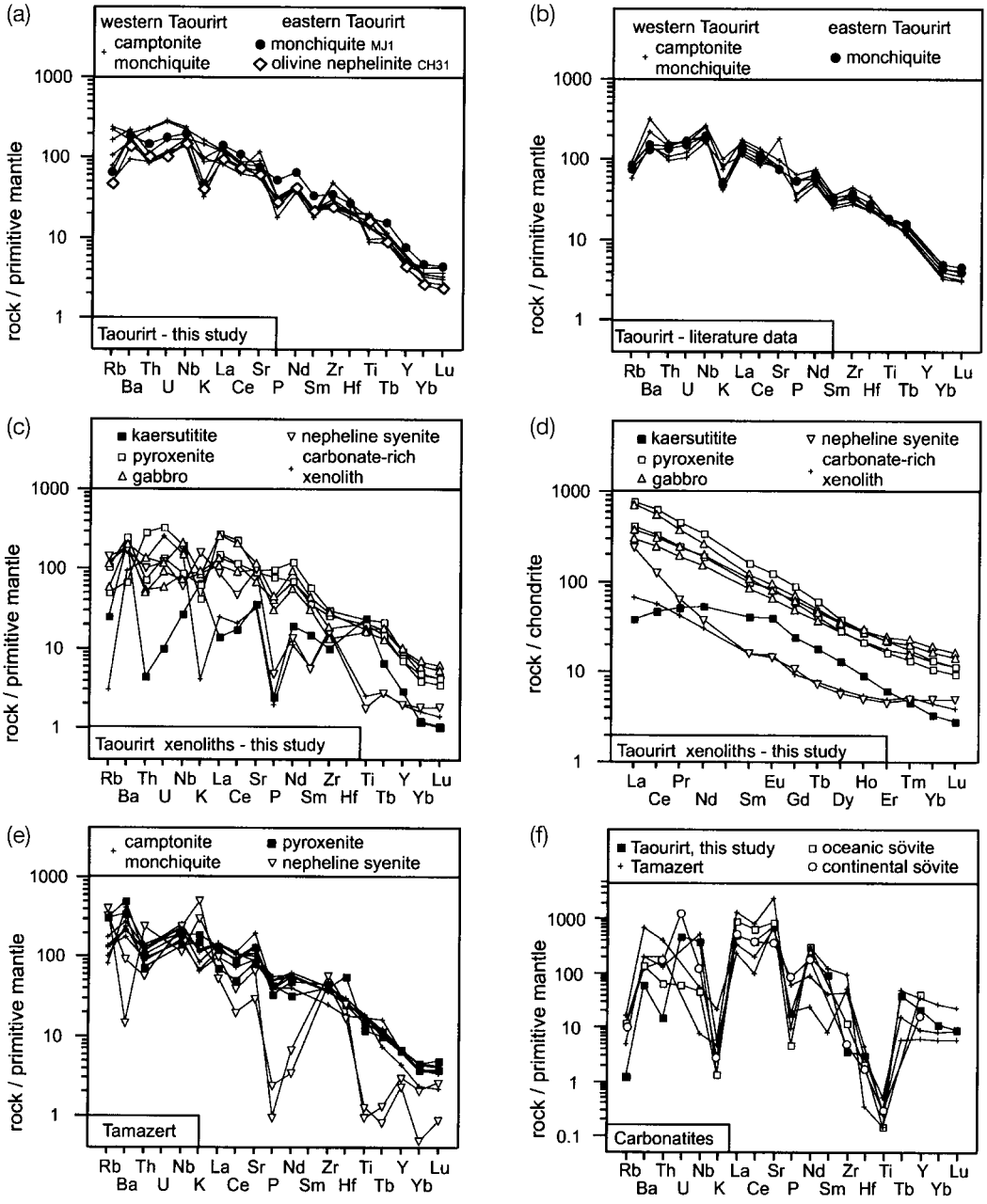


**Fig. 9.** Primitive mantle normalized trace element and REE chondrite-normalized plots for representative rocks: (a) camptonites and monchiquites (samples S2 to S6 and 93.11), monchiquite MJ1 and olivine nephelinite CH31 from this study (Table 6); (b) other lamprophyres from the Taourirt area (data source as in Fig. 8); (c) and (d) silicate xenoliths from this study; (e) data for silicate rocks from the Tamazert alkaline complex (Bouabdli, 1993); (f) the Taourirt carbonate xenolith compared with median values of continental and oceanic (Canary Islands) sövites (Le Bas, 1999) and calciocarbonatites from Tamazert (Bouabdli, 1993). The order of elements and the normalization constants are from McDonough & Sun (1995).

## The carbonate xenolith

Because the irregular dark vein network (Fig. 2f), which testifies to late-stage fluid circulation, is restricted to a few zones of the xenolith, we consider that the bulk composition of the rock has not been significantly modified. The primitive mantle normalized trace element pattern (Fig. 9f) is characterized by high Sr and LREE abundances, with enrichment factors of 600–700, and strong depletions of Rb, K and Ti. Nb and Ta abundances, which are typically hosted in

*Table 7: Nd and Sr isotopic data for Taourirt rocks*

| | | $^{87}Sr/^{86}Sr$ | $^{87}Sr/^{86}Sr_i$ | $^{43}Nd/^{144}Nd$ | $^{143}Nd/^{144}Nd_i$ |
|---|---|---|---|---|---|
| Carbonatite | 923 | 0·703014 | 0·703014 | 0·512839 | 0·512802 |
| Kaersutitite | Db | 0·703642 | 0·703591 | 0·512867 | 0·512808 |
| Pyroxenite | THD | 0·703621 | 0·703537 | 0·512837 | 0·512797 |
| Pyroxenite | THC | 0·703269 | 0·703230 | 0·512824 | 0·512787 |
| Gabbro | Scn | 0·703921 | 0·703793 | 0·512671 | 0·512627 |
| Gabbro | Scb | 0·703927 | 0·703840 | 0·512653 | 0·512610 |
| Gabbro | S43 | 0·703576 | 0·703541 | 0·512719 | 0·512683 |
| Ne-syenite | NS | 0·703846 | 0·703736 | 0·512776 | 0·512744 |
| Cxeno | ES2 | 0·704882 | 0·704875 | 0·512752 | 0·512711 |
| Host lamprophyre | S6 | 0·703504 | 0·703305 | 0·512812 | 0·512775 |
| Monchiquite | MJ1 | 0·704335 | 0·704273 | 0·512845 | 0·512805 |
| Ol-nephelinite | CH31 | 0·703411 | 0·703356 | 0·512779 | 0·512738 |

Initial $^{87}Sr/^{86}Sr_i$ and $^{143}Nd/^{144}Nd_i$ calculated at a mean age of 60 Ma. Precision of isotopic ratios is $2 \times 10^{-5}$ ($2\sigma$ level). Cxeno, carbonate-rich xenolith; Ol, olivine. Initial epsilon values were calculated with the program ISOCALC from Carroll & Rock (1991) using $(^{87}Sr/^{86}Sr)_{UR} = 0{\cdot}7045$, $(^{87}Rb/^{86}Sr)_{UR} = 0{\cdot}0816$, $(^{143}Nd/^{144}Nd)_{CHUR} = 0{\cdot}512638$ and $(^{147}Sm/^{144}Nd)_{CHUR} = 0{\cdot}1967$.

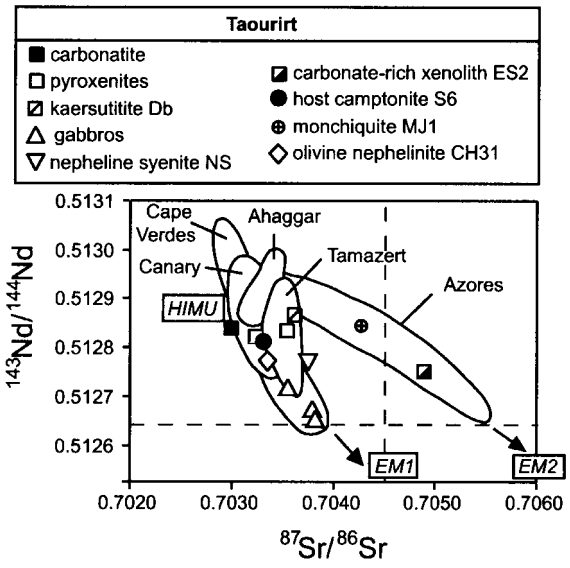


**Fig. 10.** Variation of initial $^{143}Nd/^{144}Nd$ vs $^{87}Sr/^{86}Sr$ for Taourirt rocks (Table 7), compared with data for silicate rocks from the literature (delimited fields): Tamazert (Bernard-Griffiths *et al.*, 1991); Ahaggar (Allègre *et al.*, 1981); Canary Islands (Hoernle & Tilton, 1991; Hoernle *et al.*, 1991); Cape Verdes (Gerlach *et al.*, 1988); Azores (Widom *et al.*, 1997). HIMU, EM1 and EM2 mantle components from Hofmann (1997). $2\sigma$ error bars for isotopic data (precision of $2 \times 10^{-5}$) are smaller than the symbol size. Dashed lines: Bulk Earth (BE) isotopic composition, $^{143}Nd/^{144}Nd = 0{\cdot}512638$ and $^{87}Sr/^{86}Sr = 0{\cdot}7045$.

pyrochlore, are high at 399 and 4·55 ppm, respectively. This sample exhibits an LREE-enriched chondrite-normalized profile with a steep gradient [$(La/Yb)_N = 43$; Table 6].

## Sr AND Nd ISOTOPIC DATA

Isotopic data for 10 silicate rocks and the carbonate xenolith are reported in Table 7. Sr and Nd isotopic ratios are age-corrected to the 60 Ma age of the host lamprophyres. Measured and age-corrected isotope compositions are similar and exhibit only minor variations compared with the whole range of variations.

The Nd and Sr isotope compositions of the intrusive silicate xenoliths and their host rocks plot in the depleted mantle quadrant (Fig. 10), and show a relatively large range in $^{87}Sr/^{86}Sr_i$ (0·70323–0·70384) and $^{143}Nd/^{144}Nd_i$ (0·51261 and 0·51281). The data define a linear negative trend between the most depleted samples consisting of the pyroxenite THC and the camptonite S6 to progressively more radiogenic Sr and less radiogenic Nd in the amphibole-rich gabbros (Fig. 10). The kaersutitite, pyroxenite THD and the nepheline syenite have slightly more radiogenic Sr and plot off the linear trend. The monchiquite MJ1 and the carbonate-rich xenolith ES2 have Nd isotopic compositions similar to that of pyroxenite and camptonite but higher Sr isotope ratios, and appear different from the other rock types. The isotopic composition of the carbonate xenolith is distinct ($^{143}Nd/^{144}Nd_i = 0{\cdot}51280$ and $^{87}Sr/^{86}Sr_i = 0{\cdot}70301$) from that of the silicate rocks and it plots at the most depleted end of the array, closest to the HIMU component. The trend is similar in slope to the 'LoNd' array of Hart *et al.* (1986), or the covariation termed the East African Carbonatite Line (EACL; Bell & Blenkinsop, 1987; Bell & Tilton, 2001) for young (<200 Ma) East African carbonatites.

Compared with the isotopic composition of alkaline magmatism in northern Africa, most of the Taourirt rocks (pyroxenites, kaersutitite, camptonite S6, olivine nephelinite and gabbro S43) fall within the range of composition of the Tamazert rocks (Bernard-Griffiths *et al.*, 1991), but they are very different from the Tertiary volcanics from Ahaggar, Algeria (Allègre *et al.*, 1981) (Fig. 10). Interesting analogies also exist with the alkaline magmatism in the Canary Islands, particularly with the Eocene rocks from Fuerteventura (e.g. Hoernle & Tilton, 1991, and references therein), and the Tertiary to recent magmatism of the Cape Verdes archipelago (Gerlach *et al.*, 1988). The monchiquite MJ1 and the carbonate-rich xenolith ES2 are the

only Taourirt rocks whose isotopic composition overlaps that of the young basalts from the Azores (Widom *et al.*, 1997).

## DISCUSSION

### Evidence for the Taourirt carbonatite

Concerning the carbonate xenolith, the data presented in this work and in a previous study (Mokhtari *et al.*, 1996) satisfy most of the mineralogical, chemical and isotopic criteria that characterize carbonatites (Barker, 1989). We summarize here the evidence supporting the carbonatite nature of the xenolith.

The Nd and Sr isotopic composition (Table 7) of the carbonate xenolith testifies to a depleted mantle origin and falls within the range of values known for young (<200 Ma) carbonatites (e.g. Bell & Blenkinsop, 1989; Tilton & Bell, 1994; Harmer & Gittins, 1998) (Fig. 10). The xenolith has high Sr and LREE abundances and is depleted in Rb, K and Ti, similarly to magmatic carbonatites (Kapustin, 1982; Barker, 1989; Woolley & Kempe, 1989; Le Bas, 1999).

The calcite is rich in Sr (up to 2·8 wt % SrO), which is typical of magmatic carbonatites, in contrast to replacement carbonate-rich rocks, which contain low Sr carbonates (averaging 0·08 wt % SrO; Kapustin, 1982; Ngwenya & Bailey, 1990).

Pyrochlore is a typical accessory mineral in carbonatites and despite the high variability of its chemical composition, its presence is a strong criterion to distinguish carbonatite from carbonate of sedimentary or metamorphic origin (Hogarth, 1989). Zoning during carbonate magma crystallization, either similar to that at Taourirt or the reverse, has been frequently reported in pyrochlore from different localities (Hogarth, 1989). The positive Ce anomalies in the REE profiles (Fig. 6b) are commonly observed in pyrochlore from carbonatites (e.g. Hogarth *et al.*, 1988; Hornig-Kjarsgaard, 1998). Moreover, the Nd/La ratios (~2) of the fresh yellow small grains and the rims of the zoned crystals are typical of carbonatite pyrochlores (Hogarth, 1989).

Apatite exhibits several features characteristic of apatite from carbonatites worldwide. It shows blue cathodoluminescence colours, which are typical of carbonatite apatite (Hogarth, 1989). The occurrence of two types of apatite (large zoned and small crystals) has been reported from other carbonatites, such as Oka (Girault, 1966) and Kovdor (Zaitsev & Bell, 1995). The sharp boundaries between rims and cores of the large zoned crystals (Fig. 7a) are also frequently observed in carbonatite apatite (Hogarth, 1989). The range in LREE concentrations falls within that reported for apatite from magmatic carbonatites (e.g. Hornig-Kjarsgaard, 1998; Bühn *et al.*, 2001), and the shape of the LREE pattern (negative Ce anomaly) resembles that of apatite coprecipitated with calcite in the Homa carbonatite (Bühn *et al.*, 2001). The chemical characteristics of the Taourirt apatite are similar to those reported for apatites in sövites associated with lamprophyres (Hornig-Kjarsgaard, 1998).

The granular texture of the carbonate xenolith resembles that of sövitic carbonatites. Such textures result from partial recrystallization of primary magmatic calcite crystals to form granular aggregates (Barker, 1989). This may be the case for the Taourirt carbonatite, in which a few triple junctions at the grain margins have been observed (Fig. 2f).

Thus the Taourirt rock can be considered as a carbonatite. It is a calciocarbonatite [ca-number >80, where ca-number = 100 Ca/(Ca + Mg); Table 6], which may be referred to as a sövite (Le Maître *et al.*, 1989). Its composition resembles that of the sövites from the Tamazert complex, Morocco (Bouabdli, 1993; Mourtada, 1997) and the carbonatites from the Canary Islands (Fig. 9f) (Le Bas, 1999). Many characteristics point to its similarities to early-stage rather than late-stage carbonatite magmas: (1) the Sr-rich and Mn-poor calcite is similar to that found in early sövites rather than late alvikites at Tamazert (Mourtada, 1997); (2) chemical characteristics of apatite, e.g. the low Si abundances and the REE element contents and ratios [$(La/Nd)_N = 2·2–5$; up to 1 wt % La] are close to those of apatites crystallized from early- rather than late-stage carbonatite melts (Le Bas & Handley, 1979; Bühn *et al.*, 2001), although these latter workers emphasized the diversity of the REE chemistry in apatite from sövite when considering both the abundances and the shape of the REE patterns. The range in LREE abundances of the Taourirt apatite is similar to that of apatite from shallow-level carbonatite intrusions (e.g. Kalkfeld and Ondurakorume complexes in Namibia; Bühn *et al.*, 2001).

### Petrogenesis of the carbonatite

The ultimate source of carbonatite magmas seems to lie within the convecting mantle, as their Nd, Sr and Pb isotopic compositions are similar to those of ocean island basalts (OIBs) (Le Bas & Handley, 1979; Bell & Blenkinsop, 1989; Bell, 1998; Harmer & Gittins, 1998). Nevertheless, their exact petrogenetic origin remains unclear. Carbonatite melts may be primary mantle carbonate magmas, or secondary magmas formed during the differentiation by fractional crystallization or immiscibility of an evolved parental silicate mantle melt (see references in the papers cited hereafter).

In the case of the Taourirt carbonatite, its low MgO abundance argues against a primary mantle-derived

magma, as primary carbonatites are likely to be magnesiocarbonatites (Bailey, 1993; Lee & Wyllie, 1994; Wyllie & Lee, 1998; Lee *et al.*, 2000*a*). In addition to the low MgO abundance, the carbonatite exhibits a very high $CaCO_3$ content (90%) and low total alkalis. This $CaCO_3$ content seems too high to represent a calciocarbonatite magma generated after metasomatism of wall-rock lherzolite, which produces carbonate liquids containing no more than 75–87% $CaCO_3$ (Dalton & Wood, 1993; Wyllie & Lee, 1998; Lee & Wyllie, 2000). Conversely, the Taourirt carbonatite cannot represent a liquid formed directly by immiscibility, as immiscible carbonate liquids should be rich in alkalis (Lee & Wyllie, 1994), with no more than 85% $CaCO_3$, the limit of the 'forbidden volume' of Lee & Wyllie (1998*a*, 1998*b*, 2000). Moreover, no silicate xenolith with an isotopic composition similar to that of the carbonatite has been found. A possible alternative explanation is that the Taourirt carbonatite represents a calcite-rich cumulate. Calcite crystals are known to sink rapidly and separate from their low-viscosity host carbonate magma (Wyllie & Tuttle, 1960), supporting the view that most sövitic carbonatites are cumulates (Lee & Wyllie, 1996, 1997). A calcite cumulate can crystallize from an immiscible carbonate liquid conjugate to an evolved nephelinite at low crustal pressure (Kjarsgaard, 1998), or can precipitate from magnesiocarbonatite primary magmas (Lee & Wyllie, 1994; Wyllie & Lee, 1998; Lee *et al.*, 2000*a*). At Taourirt, the precursor of the sövite cumulate remains unknown.

## Petrogenesis of the Taourirt lamprophyres

According to Rock (1991), alkaline lamprophyres are $H_2O \pm CO_2$-rich magmas generated by variable but usually rather small degree of melting of a hydrous mantle. In the case of the Taourirt lamprophyres, their Nd and Sr isotope signature and the presence of amphibole ± mica-bearing ultramafic mantle xenoliths is consistent with derivation by partial melting of a hydrous mantle source. One of the hydrous mantle xenoliths studied here (sample THC) has Nd–Sr isotopic ratios identical to that of the lamprophyre.

The normalized trace element patterns of the lamprophyres show a negative P anomaly but no anomalies in Ti and Zr (Fig. 9a). This may indicate that apatite may be a residual phase, but not zircon and ilmenite. The ranges in normalized La abundances (150–250 times chondrite) and the rather constant (4–5 times chondrite) Yb abundance are consistent with melting occurring in the garnet stability field.

Despite their Nd–Sr isotopic heterogeneity the various Taourirt lamprophyres display many similarities in their overall geochemistry, e.g. the similar strongly LREE-enriched REE patterns and substantial enrichment in incompatible elements, and the restricted range in incompatible trace element ratios. The variations observed in their major and trace element compositions could be partly explained by fractional crystallization processes. $Al_2O_3$ and total alkalis increase and CaO and $TiO_2$ decrease with differentiation (Fig. 8), whereas $Al_2O_3$/CaO and $Al_2O_3/TiO_2$ ratios remain constant for MgO > 8 wt % and then increase. These variations are consistent with fractionation processes dominated by removal of clinopyroxene ± amphibole ± Ti-magnetite. Linear trends are observed for V and Co, and to a lesser extent for Ni and Cr, if one excludes the Ni- and Cr-poor samples from the Ferme Dubois outcrops. Similarly, linear increases of some incompatible elements (e.g. U) and LREE, and the absence of variations in elemental ratios, e.g. Th/La and La/Sm, with differentiation in most samples (except samples S4 and S6), further support the prominent role of fractional crystallization in the evolution of the lamprophyres. However, the scatter of the Rb and Ba data for example (Fig. 8) implies that the magmatic evolution also involves crustal assimilation.

## Relationships between the silicate xenoliths

Some of the pyroxenite xenoliths appear to resemble liquid compositions, as deduced in previous sections on the basis of their bulk-rock chemical composition and the lack of cumulative textures. The potential links between the pyroxenite, alkali gabbro and nepheline syenite xenoliths can be evaluated through textural, chemical and isotopic data.

The major element compositions of the Taourirt rocks (Fig. 8) fall mainly within the range of compositions of the intrusive pyroxenites and nepheline syenites of Giret (1985), except for lower $Na_2O$ contents in the pyroxenites. In addition, the xenoliths plot within the range of compositions of the lamprophyres from the same area (Fig. 8). No systematic chemical variations can be found between the xenoliths (two pyroxenites, three alkali gabbros and one nepheline syenite when excluding the rocks that may be partly cumulate in origin). Pyroxenites and alkali gabbros have similar and parallel trace and REE normalized patterns (Fig. 9c and d), whereas the differently shaped REE pattern of the nepheline syenite can be attributed to the removal of apatite, titanite and amphibole, which could also explain the low $P_2O_5$, REE and $TiO_2$ contents and La/Sm ratio. However, this evidence along with the parallel REE patterns is contradicted by both the distinct incompatible trace element ratios (Table 6) and the Nd and Sr isotopic composition (Fig. 10),

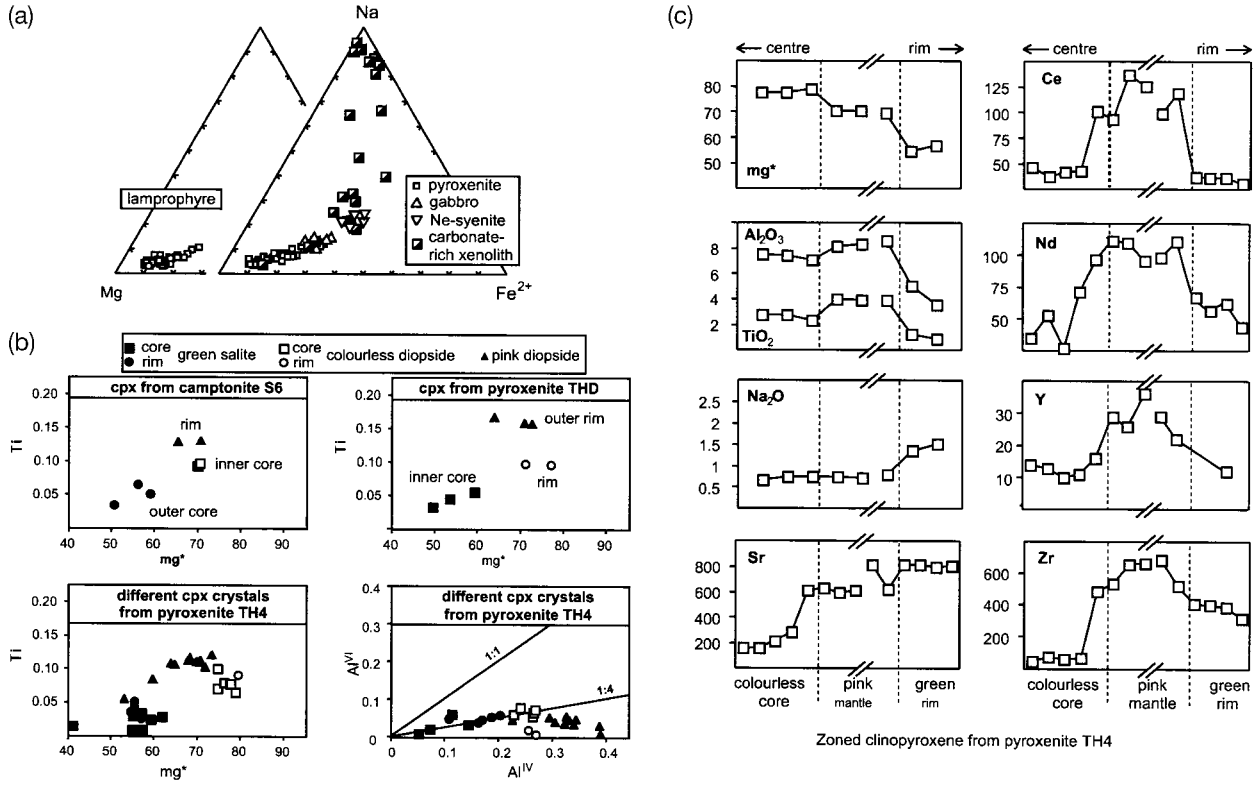


**Fig. 11.** (a) Na–Mg–$Fe^{2+}$ ternary plot of clinopyroxenes from host lamprophyres and silicate xenoliths; Ne-syenite, nepheline syenite. (b) Plots of Ti (atoms per formula unit) vs mg-number for zoned crystals from camptonite S6, pyroxenites THD and TH4, and $Al^{VI}$ vs $Al^{IV}$ distribution in zoned clinopyroxenes from pyroxenite TH4. (c) Compositional profiles from core to rim in a zoned clinopyroxene (850 μm width) from pyroxenite TH4 (Fig. 3c); major (oxide wt %) and trace (ppm) elements were determined by the electron microprobe; one analytical point every 10 μm and 15 μm for trace and major elements, respectively.

which clearly indicate that the various fragments cannot be linked to a single magmatic series. It is thus proposed that the xenoliths are unrelated to each other, and are derived from distinct mantle-derived partial melts. Moreover, the xenoliths are also unrelated to their host rocks through simple crystal–liquid fractionation processes.

## Magma mixing

Despite the progressive increase in acmite component shown by the clinopyroxenes from the pyroxenites to the nepheline syenites and the carbonate-rich rocks (Fig. 11a), which could suggest that the rocks are comagmatic, it is clear that there is little or no overlap between the various rock types. This argues against the chemical variation being an evolutionary trend. Similar 'pseudo-trends' have indeed been recognized in clinopyroxenes from alkaline complexes worldwide (Harmer, 1999).

The pyroxenes exhibit a complex chemical zoning (Figs 3 and 4). Salite and diopside occur indifferently as cores and rims, and their respective composition is identical in both cases (Fig. 11b). The cores are often resorbed; salitic cores are more resorbed than diopsidic ones, and clearly out of equilibrium with the surrounding magma. The cores represent crystals foreign to the magma that produced the overgrowths. It can be seen from the Al distribution between octahedral and tetrahedral sites (Fig. 11b) that the clinopyroxenes follow a low-pressure trend, which supports shallow-level crystallization for all the clinopyroxenes, including the cores. Therefore, it is most probable that the cores do not represent xenocrysts extracted from the wall-rock during ascent. Moreover, diopside and salite phenocrysts are present in a same rock and, as it is unlikely that a unique magma may produce both diopside and salite phenocrysts, the cores must have been introduced into the magma reservoir through magma mixing. Oscillatory zoning of diopsidic and salitic compositions suggests repeated mixing episodes. This is further supported by compositional profiles recorded in a number of different crystals from core to rim, which exhibit abrupt chemical variations for both major and trace elements even in the case of normally zoned (i.e. with decreasing mg-number towards the rim) crystals

(Fig. 11c). In these same crystals the zoning appears optically continuous, although back-scattered electron images reveal resorbed contacts between the zones. Similar zoning features have been reported in clinopyroxenes from various alkaline igneous complexes (e.g. Bédard *et al.*, 1988; Dobosi & Fodor, 1992; Simonetti *et al.*, 1996; Neumann *et al.*, 1999, and references therein), and have been linked to open-system behaviour, such as magma mixing events involving distinct pulses of more or less fractionated magmas. The fact that both diopside and salite cores are present indicates that mixing occurred subsequent to the crystallization of both types of clinopyroxenes in their respective magmas. The latter may have occurred in different magma chambers or in a single stratified reservoir. Magma mixing or stirring, capable of creating a turbulent regime and disrupting any compositional and thermal gradient (Turner & Campbell, 1986), could have been enhanced by the volatile-rich nature of the Taourirt magmas.

Some of the zoned clinopyroxenes have recorded up to four cycles of crystallization interrupted by episodes of mixing between evolved and more mafic melts. Such processes have been described as 'fractional crystallization in periodically refilled magma chambers (FCM processes)' by Neumann *et al.* (1999). According to those workers, decoupling of major and trace elements occurs during this process, and is evidenced by: (1) the zoned clinopyroxene from pyroxenite TH4 (Table 4), which has a strong enrichment in LREE for only a minor decrease in mg-number between the colourless diopside core and the pinkish mantling diopside; (2) the lack of correlation between incompatible element (La) and mg-number (not shown).

The high Zr/Sm and low La/Yb ratios in most salites compared with those in diopside (Table 4) may be attributed to syn-crystallization of apatite and salite (evident in some pyroxenites), but may also suggest a distinct trace element composition for the liquids parental to diopside and salite. It may be linked to the abundance of carbonate in the liquids and possible immiscibility phenomena (i.e. separation of a carbonate liquid with very low Zr/Sm ratio thus leading to high Zr/Sm ratio in the residual silicate liquid).

## Source characteristics

The Nd and Sr isotope compositions of the Taourirt silicate rocks indicate that their parental magmas were derived from a long-term LREE- and Rb-depleted mantle source, which is the case for many carbonatite complexes worldwide (Bell & Blenkinsop, 1989; Bell, 1998). The volatile-rich nature of the Taourirt rocks (e.g. carbonatite and lamprophyres) and their high abundances in incompatible trace elements require the presence of a metasomatized mantle, and thus a refertilization of the mantle source before the partial melting event. As there is no correlation between the degree of incompatible element enrichment and the isotopic signatures, the metasomatic episode was probably recent, which is typical of many alkaline provinces (Allègre *et al.*, 1981).

Given its Nd and Sr isotopic composition, distinct from that of any of the surrounding silicate rocks, the Taourirt carbonatite is considered to have been derived from a parental magma distinct from that which gave rise to the silicate rocks. Similarly, the Taourirt silicate rocks themselves cannot represent a suite simply related through closed-system magmatic processes, and the silicate xenoliths have to represent fragments derived from separate and unrelated intrusions.

Alternative processes that can explain such large isotopic variations involve combined assimilation and fractional crystallization (AFC, De Paolo, 1981), or mixing between several distinct mantle and/or crustal components. No correlation was observed between $^{143}Nd/^{144}Nd$ ratios and $SiO_2$ abundances, which precludes a binary mixing between a depleted mantle component and a crustal component, during an AFC process. Moreover, such a simple mixing would not generate the array observed in the Nd–Sr isotope plot (Fig. 10). In addition, there is no correlation between $^{87}Sr/^{86}Sr$ and $SiO_2$ or any other major elements or trace element ratios (e.g. Rb/Sr, Sm/Nd, Nb/U, K/U). The assimilation of lower crust fails to explain most of the observed data, even if complex models of crustal assimilation (AFC) cannot be entirely ruled out. However, the lack of knowledge of the parental magma and of appropriate partition coefficients does not allow us to accurately assess this hypothesis.

Mixing of mantle melts, which is an alternative model to explain the variation in isotopic data, is a plausible model for the Taourirt rocks, although additional complexity may have been brought about by crustal contamination in some samples (Figs 8 and 10). In a mixing model, the depleted and enriched melts relative to the Bulk Earth isotopic composition may correspond to HIMU-type and EM-type components, respectively, as proposed by several workers to account for the Sr and Nd isotopic variations of carbonatites worldwide (e.g. Bell, 1998; Bell & Tilton, 2001), even if no Pb isotope data are available for Taourirt rocks to confirm this. The physical location of the mantle components may be the subcontinental lithosphere as initially proposed by Hart *et al.* (1986), or a plume (HIMU component) may have interacted with the lithosphere (EM component); Bell & Tilton (2001) recently proposed that both the HIMU and EM1 components are contained within an isotopically heterogeneous plume

that originates in the lower mantle. The direct or indirect role of mantle plumes has been proposed for the genesis of the carbonatite alkaline complexes from the Canary Islands (Hoernle & Tilton, 1991; Hoernle *et al*., 1991) and the Cape Verdes archipelago (Gerlach *et al*., 1988), and similarly invoked by Bell & Simonetti (1996) and Bell & Tilton (2001) to explain the isotope systematics of the young East African carbonatites; these latter workers assumed that 'many, perhaps all, carbonatites are related to plume activity'. The most depleted Taourirt rocks, i.e. the carbonatite, one pyroxenite and the host lamprophyre, plot within the field defined by the most plume-like magmatic rocks from the Canary Islands (Hoernle & Tilton, 1991), whereas the olivine nephelinite and the gabbros plot along a trend towards the enriched EM1-type component (Fig. 10), a trend similar to that shown by the rocks from the Canary Islands and the Cape Verdes (Gerlach *et al*., 1988), and the Tamazert alkaline complex (Bernard-Griffiths *et al*., 1991). The monchiquite MJ1 has a higher Sr isotopic ratio and falls within the range of the Azores OIB, which may suggest the involvement of an EM2-like source component (Widom *et al*., 1997). According to Widom *et al*., this component may correspond to hydrous metasomatized mantle (phlogopite and phlogopite K-richterite peridotite, PP and PKP, respectively) and MARID (mica, amphibole, rutile, ilmenite and diopside) suite rocks (Erlank *et al*., 1987; Hawkesworth *et al*., 1990). This could be a plausible explanation for some of Taourirt lamprophyres, which have a low Ba/Nb ratio (9–10) similar to that of the PP, PKP and MARID rocks. In addition, PKP and MARID xenoliths have been found in lamprophyres (e.g. MJ1) and olivine nephelinites from the eastern part of the Taourirt area (Wagner *et al*., 1996).

## CONCLUSION

Mineralogical, geochemical and isotopic data are reported for the main rock types at Taourirt, which include a calciocarbonatite and alkaline silicate rocks (pyroxenites, melteigites, kaersutitites, gabbros, nepheline syenites) known only as xenoliths in monchiquites and camptonites. The main conclusions are summarized below.

(1) Mineralogical characteristics (e.g. the association of pyrochlore and apatite) and trace element and isotopic compositions support the carbonatitic nature of the carbonate xenolith from Taourirt. It is a calciocarbonatite, which probably represents a cumulate from an unknown magmatic precursor.

(2) Trace element relationships and contrasting Nd–Sr isotopic compositions argue against the carbonatite being derived by magmatic differentiation from parental magmas similar to any of the samples collected. Conversely, the silicate xenoliths appear to be fragments from several unrelated intrusions, and are themselves unrelated to their host lamprophyres. This may indeed be the case in many so-called alkaline–carbonatite complexes worldwide (Harmer & Gittins, 1998).

(3) The major and trace element compositions of the host alkaline lamprophyres suggest that fractional crystallization is not the only process involved in the petrogenesis of these rocks. Moreover, the complex zoning of the clinopyroxenes from both the lamprophyres and the silicate xenoliths further supports open-system behaviour and requires repeated mixing episodes of batches of more or less fractionated magmas. The model of several cycles of fractional crystallization interrupted by episodes of mixing in magma reservoirs with periodic replenishment (Neumann *et al*., 1999) is likely to account for the observed data.

(4) Initial Sr–Nd isotopic compositions of the various xenolith types plot in the depleted quadrant of the Nd–Sr isotope diagram. The large variation documented by the isotopic data and the lack of evidence for crustal interaction suggest the presence of a heterogeneous mantle involving HIMU and EM components. The carbonatite has the least enriched Nd–Sr isotopic signature, close to the HIMU mantle end-member. The silicate rocks may represent discrete partial melting episodes representing variable contributions of the HIMU and EM components. The HIMU or both HIMU and EM1 components may be related to plume activity, as proposed by Simonetti *et al*. (1998) and Bell & Tilton (2001) for many carbonatite provinces. The EM2 mantle component may also be involved to explain the Nd–Sr isotope systematics of some samples.

## ACKNOWLEDGEMENTS

We thank A. Cheilletz (CRPG, Nancy) for the mica dating; D. Garcia (ENSMSE, Saint-Étienne), J. Samuel and R. Rouault (CGS, Strasbourg) for the whole-rock ICP-AES analyses; M. Steinmann, B. Kiefel and D. Tisserant (CGS, Strasbourg) for their help in the Sr–Nd isotopic analysis; and M. Fialin (CAMPARIS, Paris 6) for electron microprobe improvements allowing trace element analysis. We thank also M. Fonteilles and D. Velde (UPMC, Paris) for helpful discussions, and G. M. Yaxley (University of Tasmania, Tasmania) for having reviewed an early stage of this work. We are grateful

to A. Simonetti (GEOTOP, Montréal) and R. E. Harmer (Council for Geoscience, Pretoria), who made thorough reviews and provided stimulating comments, and to M. Wilson (School of Earth Sciences, Leeds) for many pertinent suggestions that improved the paper. Mike Toplis (CRPG, Nancy) was kind enough to correct the English of the whole manuscript.

## REFERENCES

Agard, J. (1950). L'âge et le mode de gisement des aïounites et mestigmérites du Maroc oriental. *Notes du Service Géologique du Maroc* **76**, 189–195.

Agard, J., Emberger, A. & Saadi, M. (1980). Le cadre géologique des minéralisations du Maroc. *Notes et Mémoires du Service Géologique du Maroc* **276**, 21–35.

Aghchmi, E. M. (1984). Les carbonatites filoniennes de l'Oued Tamazeght et leurs relations avec les métasyénites (Haut-Atlas de Midelt, Maroc). 3ème Cycle Thesis, Université Paul Sabatier, Toulouse, 106 pp.

Allègre, C. J., Dupré, B., Lambret, B. & Richard, P. (1981). The subcontinental versus suboceanic debate. I. Lead–neodymium–strontium isotopes in primary alkali basalts from a shield area: the Ahaggar volcanic suite. *Earth and Planetary Science Letters* **52**, 85–92.

Bailey, D. K. (1993). Carbonate magmas. *Journal of the Geological Society, London* **150**, 637–651.

Barker, D. S. (1989). Field relations of carbonatites. In: Bell, K. (ed.) *Carbonatites: Genesis and Evolution*. London: Unwin Hyman, pp. 38–69.

Beccaluva, L., Barbieri, M., Born, H., Brotzu, P., Coltorti, M., Conte, A., Garbarino, C., Gomes, C. B., Macciotta, G., Morbidelli, L., Ruberti, E., Siena, F. & Traversa, G. (1992). Fractional crystallization and liquid immiscibility processes in the alkaline–carbonatite complex of Juquia (São Paulo, Brazil). *Journal of Petrology* **33**, 1371–1404.

Bédard, J. H. J., Don Francis, M. & Ludden, J. (1988). Petrology and pyroxene chemistry of Monteregian dykes: the origin of concentric zoning and green cores in clinopyroxenes from alkali basalts and lamprophyres. *Canadian Journal of Earth Sciences* **25**, 2041–2058.

Bell, K. (1998). Radiogenic isotope constraints on relationships between carbonatites and associated silicate rocks—a brief review. *Journal of Petrology* **39**, 1987–1996.

Bell, K. & Blenkinsop, J. (1987). Nd and Sr isotopic compositions of East African carbonatites: implications for mantle heterogeneity. *Geology* **15**, 99–102.

Bell, K. & Blenkinsop, J. (1989). Neodymium and strontium isotope geochemistry of carbonatites. In: Bell, K. (ed.) *Carbonatites: Genesis and Evolution*. London: Unwin Hyman, pp. 278–300.

Bell, K. & Simonetti, A. (1996). Carbonatite magmatism and plume activity: implications from the Nd, Pb and Sr isotope systematics of Oldoinyo Lengai. *Journal of Petrology* **37**, 1321–1339.

Bell, K. & Tilton, G. R. (2001). Nd, Pb and Sr isotopic compositions of East African carbonatites: evidence for mantle mixing and plume inhomogeneity. *Journal of Petrology* **42**, 1927–1945.

Bernard-Griffiths, J., Fourcade, S. & Dupuy, C. (1991). Isotopic study (Sr, Nd, O and C) of lamprophyres and associated dykes from Tamazert (Morocco): crustal contamination processes and source characteristics. *Earth and Planetary Science Letters* **103**, 190–199.

Bouabdli, A. (1993). Pétrologie et géochimie du complexe alcalin de Tamazert (Haut-Atlas de Midelt). Rôle des carbonates 3ème Cycle Thesis, University Ibn Tofail, Kenitra, Morocco, 198 pp.

Bouabdli, A., Dupuy, C. & Dostal, J. (1988). Geochemistry of Mesozoic alkaline lamprophyres and related rocks from the Tamazert massif, High Atlas (Morocco). *Lithos* **22**, 43–58.

Bühn, B., Wall, F. & Le Bas, M. J. (2001). Rare-earth element systematics of carbonatitic fluorapatites, and their significance for carbonatite magma evolution. *Contributions to Mineralogy and Petrology* **141**, 572–591.

Carroll, G. W. & Rock, N. M. S. (1991). ISOCALC: a simple Rb–Sr and Sm–Nd isotopic calculator for the Apple Macintosh. *Computers and Geosciences* **17**, 465–467.

Chabiron, A., Alyoshin, A. P., Cuney, M., Deloule, E., Golubev, V. N., Velitchkin, V. I. & Poty, B. (2001). Geochemistry of the rhyolitic magmas from the Streltsovka caldera (Transbaikalia, Russia): a melt inclusion study. *Chemical Geology* **175**, 273–290.

Charlot, R., Choubert, G., Faure-Muret, A. & Hamel, C. (1964). Age des aïounites du Maroc Nord-Oriental. *Comptes Rendus Sommaire de la Société Géologique de France* **9**, 401–402.

Dalton, J. A. & Wood, B. J. (1993). The compositions of primary carbonate melts and their evolution through wallrock reaction in the mantle. *Earth and Planetary Science Letters* **119**, 511–525.

De Paolo, D. J. (1981). Trace element and isotopic effects of combined wall-rock assimilation and fractional crystallization. *Earth and Planetary Science Letters* **53**, 189–202.

Dobosi, G. & Fodor, R. V. (1992). Magma fractionation, replenishment, and mixing as inferred from green-core clinopyroxenes in Pliocene basanite, southern Slovakia. *Lithos* **28**, 133–150.

Duparc, L. (1925). Sur quelques roches filoniennes curieuses des environs de Mestigmer (Maroc). *Comptes Rendus de l'Académie des Sciences* **152**, 1764–1766.

Edgar, A. D. (1974). On the use of the term 'Agpaitic'. *Mineralogical Magazine* **39**, 729–730.

Erlank, A. J., Waters, F. G., Hawkesworth, C. J., Haggerty, S. E., Allsopp, H. L., Rickard, R. S. & Menzies, M. A. (1987). Evidence for mantle metasomatism in peridotite nodules from the Kimberley Pipes, South Africa. In: Menzies, M. A. & Hawkesworth, C. J. (eds) *Mantle Metasomatism*. London: Academic Press, pp. 221–311.

Gerlach, D., Cliff, R. A., Davies, G. R., Norry, M. & Hodgson, N. (1988). Magma sources of the Cape Verdes archipelago: isotopic and trace element constraints. *Geochimica et Cosmochimica Acta* **52**, 2979–2992.

Girault, J. (1966). Genèse et géochimie de l'apatite et de la calcite dans les roches liées au complexe carbonatitique et hyperalcalin d'Oka (Canada). *Bulletin de la Société française de Minéralogie et Cristallographie* **89**, 496–513.

Giret, P. (1985). Histoire paléogéographique, pétrologique et structurale du district à fluorine de Taourirt. 3ème Cycle Thesis, University of Orléans, 191 pp.

Govindaraju, K. (1989), Compilation of working values and sample description for 272 geostandards. *Geostandards Newsletter* **13**, 1–113.

Harmand, D. & Cantagrel, J. M. (1984). Le volcanisme alcalin Tertiaire et Quaternaire du Moyen Atlas (Maroc): chronologie K/Ar et cadre géodynamique. *Journal of African Earth Sciences* **2**, 51–55.

Harmer, R. E. (1999). The petrogenetic association of carbonatite and alkaline magmatism: constraints from the Spitskop Complex, South Africa. *Journal of Petrology* **40**, 525–548.

Harmer, R. E. & Gittins, J. (1998). The case for primary, mantle-derived carbonatite magma. *Journal of Petrology* **39**, 1895–1903.

Hart, S. R., Gerlach, D. C. & White, W. M. (1986). A possible new Sr–Nd–Pb mantle array and consequences for mantle mixing. *Geochimica et Cosmochimica Acta* **50**, 1551–1557.

Hawkesworth, C., Erlank, A. J., Kempton, P. D. & Waters, F. G. (1990). Mantle metasomatism: isotope and trace element trends in xenoliths from Kimberley, South Africa. *Chemical Geology* **85**, 19–34.

Hernandez, J., Leblanc, D. & Marçais, J. (1976). Une manifestation volcanique d'âge paléocène dans le Rif (Maroc): les laves basaltiques de Sidi Maatoug. *Bulletin de la Société Géologique Française* **XVIII**(7), 697–705.

Hoernle, K. & Tilton, G. (1991). Sr–Nd–Pb isotope data for Fuerteventura (Canary Islands) basal complex and subaerial volcanics: applications to magma genesis and evolution. *Schweizerisches Mineralogisches Mitteilungen* **71**, 3–18.

Hoernle, K., Tilton, G. & Schmincke, H.-U. (1991). Sr–Nd–Pb isotopic evolution of Gran Canaria: evidence for shallow enriched mantle beneath the Canary Islands. *Earth and Planetary Science Letters* **106**, 44–63.

Hofmann, A. W. (1997). Mantle geochemistry: the message from oceanic volcanism. *Nature* **385**, 219–229.

Hogarth, D. D. (1989). Pyrochlore, apatite and amphibole: distinctive minerals in carbonatite. In: Bell, K. (ed.) *Carbonatites: Genesis and Evolution*. London: Unwin Hyman, pp. 105–148.

Hogarth, D. D., Rushforth, P. & McCorkell, R. H. (1988). The Blackburn carbonatites, near Ottawa, Ontario: dykes with fluidized emplacement. *Canadian Mineralogist* **26**, 377–390.

Hornig-Kjarsgaard, I. (1998). Rare-earth elements in sövitic carbonatites and their mineral phases. *Journal of Petrology* **39**, 2105–2122.

Kapustin, Y. L. (1982). Geochemistry of strontium and barium in carbonatites. *Geokhimiya* **3**, 399–382 (in Russian).

Kjarsgaard, B. A. (1998). Phase relations of a carbonated high-CaO nephelinite at 0·2 and 0·5 GPa. *Journal of Petrology* **39**, 2061–2075.

Laville, E. (1981). Rôle des décrochements dans le mécanisme de formation des bassins d'effondrement du Haut Atlas marocain au cours des temps triasique et liasique. *Bulletin de la Société géologique de France* **3**, 303–312.

Laville, E. & Piqué, A. (1991). La distension crustale atlantique et atlasique au maroc au début du Mésosoïque: le rejeu de structures hercyniennes. *Bulletin de la Société géologique de France* **162**, 1161–1171.

Le Bas, M. J. (1987). Nephelinites and carbonatites. In: Fitton, J. G. & Upton, B. G. (eds) *Alkaline Igneous Rocks*. *Geological Society, London, Special Publications* **30**, 53–83.

Le Bas, M. J. (1999). Sövite and alvikite: two chemically distinct carbonatites C1 and C2. *South African Journal of Geology* **102**, 109–121.

Le Bas, M. J. & Handley, C. D. (1979). Variation in apatite composition in ijolitic and carbonatitic igneous rocks. *Nature* **279**, 54–56.

Le Maître, R. W., Bateman, P., Didek, A., Keller, J., Lameyre, J., Le Bas, M. J., Sabine, P. A., Sorensen, H., Streckeisen, A., Woolley, A. R. & Zanettin, B. (1989). *A Classification of Igneous Rocks and Glossary of Terms*. Oxford: Blackwell, 193 pp.

Lee, W.-J. & Wyllie, P. J. (1994). Experimental data bearing on liquid immiscibility, crystal fractionation, and the origin of calciocarbonatites and natrocarbonatites. *International Geology Review* **36**, 797–819.

Lee, W.-J. & Wyllie, P. J. (1996). Liquid immiscibility in the join $NaAlSi_3O_8$–$CaCO_3$ to 2·5 GPa and the origin of calciocarbonatite magmas. *Journal of Petrology* **37**, 1125–1152.

Lee, W.-J. & Wyllie, P. J. (1997). Liquid immiscibility between nephelinite and carbonatite from 1·0 to 2·5 GPa compared with mantle compositions. *Contributions to Mineralogy and Petrology* **127**, 1–16.

Lee, W.-J. & Wyllie, P. J. (1998*a*). Processes of crustal carbonatite formation by liquid immiscibility and differentiation, elucidated by model systems. *Journal of Petrology* **39**, 2005–2013.

Lee, W.-J. & Wyllie, P. J. (1998*b*). Petrogenesis of carbonatite magmas from mantle to crust, constrained by the system CaO–(MgO + FeO*)–($Na_2O$ + $K_2O$)–($SiO_2$ + $Al_2O_3$ + $TiO_2$)–$CO_2$. *Journal of Petrology* **39**, 495–517.

Lee, W.-J. & Wyllie, P. J. (2000). The system CaO–MgO–$SiO_2$–$CO_2$ at 1 GPa, metasomatic wehrlites, and primary carbonatite magmas. *Contributions to Mineralogy and Petrology* **138**, 214–228.

Lee, W.-J., Fanelli, M. F., Cava, N. & Wyllie, P. J. (2000*a*). Calciocarbonatite and magnesiocarbonatite rocks and magmas represented in the system CaO–MgO–$CO_2$–$H_2O$ at 0·2 GPa. *Mineralogy and Petrology* **68**, 225–256.

Lee, W.-J., Huang, W. L. & Wyllie, P. J. (2000*b*). Melts in the mantle modeled in the system CaO–MgO–$SiO_2$–$CO_2$ at 2·7 GPa. *Contributions to Mineralogy and Petrology* **138**, 199–213.

Mattauer, M., Tapponier, P. & Proust, F. (1977). Sur les mécanismes de formation des chaînes intracontinentales. L'exemple des chaînes atlasiques du Maroc. *Bulletin de la Société géologique de France* **XIX**(3), 521–526.

McDonough, W. F. & Sun, S.-s. (1995). The composition of the Earth. *Chemical Geology* **120**, 223–253.

Mokhtari, A. (1995). Etude pétrologique et minéralogique des roches alcalines Eocène (monchiquites, camptonites et néphélinites) et de leurs enclaves mantelliques et alcalines (carbonatite, pyroxénites et syénites) de la région de Taourirt (Maroc oriental). 3ème Cycle Thesis, University Moulay Ismail, Meknès, Morocco, 181 pp.

Mokhtari, A. & Velde, D. (1988). Xenocrysts in Eocene camptonites from Taourirt, northern Morocco. *Mineralogical Magazine* **52**, 587–601.

Mokhtari, A., Wagner, C. & Velde, D. (1996). Découverte d'une enclave de carbonatite dans une camptonite de Taourirt (Nord-Est du Maroc). Conséquences géologiques. *Compte Rendus de l'Académie des Sciences, Série IIa* **323**, 467–474.

Mourtada, S. (1997). Pétrogenèse des carbonatites et contribution à l'étude des minéralisations associées: exemple du complexe alcalin de Tamazert Haut-Atlas marocain). 3ème Cycle Thesis, University Blaise Pascal, Clermont-Ferrand, 320 pp.

Nelson, D. R., Chivas, A. R., Chappell, B. W. & McCulloch, M. T. (1988). Geochemical and isotopic systematics in carbonatites and implications for the evolution of the ocean-island sources. *Geochimica et Cosmochimica Acta* **52**, 1–17.

Neumann, E.-R., Wulff-Pedersen, E., Simonsen, S. L., Pearson, N. J., Marti, J. & Mitjavila, J. (1999). Evidence of fractional crystallization of periodically refilled magma chambers in Tenerife, Canary Islands. *Journal of Petrology* **40**, 1089–1123.

Ngwenya, B. T. & Bailey, D. K. (1990). Kaluwe carbonatite, Zambia: an alternative to natrocarbonatite. *Journal of the Geological Society, London* **147**, 213–216.

Pouchou, J.-L. & Pichoir, F. (1985). 'PAP' ($\phi$–$\rho$–$\chi$) correction procedure for improved quantitative microanalysis. In: Armstrong, J. T. (ed.) *Microbeam Analysis*. San Francisco, CA: San Francisco Press, pp. 104–106.

Rock, N. M. S. (1991). *Lamprophyres*. Glasgow: Blackie, 285 pp.

Simonetti, A. & Bell, K. (1994). Nd, Pb and Sr isotopic data from the Napak carbonatite–nepheline centre, eastern Uganda: an example of open-system crystal fractionation. *Contributions to Mineralogy and Petrology* **115**, 356–366.

Simonetti, A., Shore, M. & Bell, K. (1996). Diopside phenocrysts from nephelinite lavas, Napak volcano, Eastern Uganda: evidence for magma mixing. *Canadian Mineralogist* **34**, 411–421.

Simonetti, A., Goldstein, S. I., Schmidberger, S. S. & Viladkar, S. G. (1998). Geochemical and Nd, Pb, and Sr isotope data from

Dekkan alkaline complexes—inferences for mantle sources and plume–lithosphere interaction. *Journal of Petrology* **39**, 1847–1864.

Steinmann, M. & Stille, P. (1997). Rare earth element behavior and Pb, Sr and Nd isotope systematics in a heavy metal contaminated soil. *Applied Geochemistry* **12**, 607–623.

Sweeney, R. J. (1994). Carbonatite melt compositions in the earth's mantle. *Earth and Planetary Science Letters* **128**, 259–270.

Tilton, G. R. & Bell, K. (1994). Sr–Nd–Pb isotope relationships in Late Archean carbonatites and alkaline complexes: applications to the geochemical evolution of Archean mantle. *Geochimica et Cosmochimica Acta* **58**, 3145–3154.

Tisserant, D., Thuizat, R. & Agard, J. (1976). Données géochronologiques sur le complexe de roches alcalines du Tamazeght (Haut-Atlas-de-Midelt, Maroc). *Bulletin du BRGM, Section II* **3**, 279–283.

Tricca, A., Stille, P., Steinmann, M., Kiefel, B., Samuel, J. & Eikenberg, J. (1999). Rare earth elements and Sr and Nd isotopic compositions of dissolved and suspended loads from small river systems in the Vosges Mountains (France). *Chemical Geology* **160**, 139–158.

Turner, J. S. & Campbell, I. H. (1986). Convection mixing in magma chambers. *Earth-Science Reviews* **23**, 255–352.

Wagner, C., Mokhtari, A. & Velde, D. (1993). Xenocrystic richterite in an olivine-nephelinite: destabilisation and diffusion phenomena. *Mineralogical Magazine* **57**, 515–525.

Wagner, C., Deloule, E. & Mokhtari, A. (1996). Richterite-bearing peridotites and MARID type inclusions in lavas from north eastern Morocco: mineralogy and D/H isotopic studies. *Contributions to Mineralogy and Petrology* **124**, 406–421.

Widom, E., Carlson, R. W., Gill, J. B. & Schmincke, H.-U. (1997). The Sr–Nd–Pb isotope and trace element evidence for the origin of the São Miguel, Azores enriched mantle source. *Chemical Geology* **140**, 49–68.

Woolley, A. R. & Kempe, D. R. C. (1989). Carbonatites: nomenclature, average chemical compositions, and element distribution. In: Bell, K. (ed.) *Carbonatites: Genesis and Evolution*. London: Unwin Hyman, pp. 1–14.

Wyllie, P. J. & Lee, W.-J. (1998). Model system controls on conditions for formation of magnesiocarbonatite and calciocarbonatite magmas from the mantle. *Journal of Petrology* **39**, 1885–1893.

Wyllie, P. J. & Tuttle, O. F. (1960). The system $CaO–CO_2–H_2O$ and the origin of carbonatites. *Journal of Petrology* **1**, 1–46.

Zaitzev, A. & Bell, K. (1995). Sr and Nd isotope data of apatite, calcite and dolomite as indicators of source, and the relationships of phoscorites and carbonatites from the Kovdor massif, Kola peninsula, Russia. *Contributions to Mineralogy and Petrology* **121**, 324–335.